ANNUAL REVIEWS

Annual Review of Nuclear and Particle Science

Neutrinoless Double-Beta Decay: Status and Prospects

Michelle J. Dolinski,[1] Alan W.P. Poon,[2] and Werner Rodejohann[3]

[1]Department of Physics, Drexel University, Philadelphia, Pennsylvania 19104, USA; email: dolinski@drexel.edu

[2]Institute for Nuclear and Particle Astrophysics, Nuclear Science Division, Lawrence Berkeley National Laboratory, Berkeley, California 94720, USA; email: awpoon@lbl.gov

[3]Max-Planck-Institut für Kernphysik, 69029 Heidelberg, Germany; email: werner.rodejohann@mpi-hd.mpg.de

Annu. Rev. Nucl. Part. Sci. 2019. 69:219–51

First published as a Review in Advance on August 6, 2019

The *Annual Review of Nuclear and Particle Science* is online at nucl.annualreviews.org

https://doi.org/10.1146/annurev-nucl-101918-023407

Keywords

lepton-number violation, neutrinos, beyond the Standard Model

Abstract

Neutrinoless double-beta decay is a forbidden, lepton-number-violating nuclear transition whose observation would have fundamental implications for neutrino physics, theories beyond the Standard Model, and cosmology. In this review, we summarize the theoretical progress to understand this process, the expectations and implications under various particle physics models, and the nuclear physics challenges that affect the precise predictions of the decay half-life. We also provide a synopsis of the current and future large-scale experiments that aim to discover this process in physically well-motivated half-life ranges.

Contents

1. INTRODUCTION

The discoveries of neutrino oscillations, adiabatic lepton flavor transformation, and neutrino mass (1–5) furnished the first evidence of physics beyond the Standard Model (SM). Much is still to be learned about the neutrinos: the mass-generation mechanism, the absolute mass scale, the *CP*-transformation properties, and the question of whether they are Majorana fermions (6). The resolution of these unknowns would extend our understanding of not only the underlying symmetries that govern leptons but also baryogenesis and the evolution of the Universe. If the SM-forbidden neutrinoless double-beta ($0\nu\beta\beta$) decay process were observed, it would directly confirm lepton-number violation and the Majorana nature of neutrinos (7). Depending on the assumed mechanism, vital information about the underlying model parameters could be obtained. Interestingly, the range of possible models for $0\nu\beta\beta$ decay extends from sub-eV neutrinos to multi-TeV heavy particles, leading to a variety of potential consequences for particle physics and cosmology. Without assuming any particular driving decay mechanism, the searches for $0\nu\beta\beta$ decay are searches for lepton-number violation whose observation would demonstrate the breaking of a global conservation law of the SM. These fundamental implications are the motivation for the prodigious activities in the searches for experimental evidence and theoretical underpinnings of this process.

Double-beta ($\beta\beta$) decay is an isobaric transition from a parent nucleus (A, Z) to a daughter nucleus $(A, Z+2)$ two nuclear charges away. In the two-neutrino double-beta ($2\nu\beta\beta$) decay mode,

two electrons and two electron-type antineutrinos accompany the transition (8):

$$(A, Z) \rightarrow (A, Z+2) + 2\, e^- + 2\, \bar{\nu}_e + Q_{\beta\beta}, \qquad 1.$$

where $Q_{\beta\beta}$ is the energy released. It is an SM-allowed second-order weak decay with a typical half-life of $>10^{19}$ years. This decay mode was first deduced in a radiochemical experiment in 1950 (9) and subsequently observed in real time in a dozen nuclei since the first laboratory measurement in the late 1980s (10, 11). The readers are referred to a previous article in this journal (12) for a comprehensive review.

No neutrinos are emitted in the SM-forbidden $0\nu\beta\beta$-decay mode:

$$(A, Z) \rightarrow (A, Z+2) + 2\, e^- + Q_{\beta\beta}, \qquad 2.$$

in which the lepton number is violated by two units ($\Delta L = 2$). The experimental search for this decay is extremely challenging, and all previous attempts have returned empty-handed with the best current half-life limits of $>10^{26}$ years. The experimental difficulties are matched by the theoretical ones; in particular, understanding the nuclear physics aspects of the decay has been a persistent challenge.

There have been a number of review articles on $0\nu\beta\beta$ decay (e.g., 13–16). Our goal in this review is to capture some of the more recent theoretical and experimental developments, as the current experiments have reached a $0\nu\beta\beta$-decay half-life ($T^{0\nu}_{1/2}$) limit in the range of 10^{25}–10^{26} years, and a worldwide program to search for this decay with two orders of magnitude of improvement in sensitivity is being pursued.

This article is organized as follows. Section 2 provides the particle physics motivations for the search for $0\nu\beta\beta$ decay. The discussion focuses on the association of $0\nu\beta\beta$ decay with lepton-number violation and neutrino mass, as well as the mechanisms that could precipitate the decay. The interpretation of the observed signal would require knowledge of the nuclear transition between the initial and final states. The focus of Section 3 is on the nuclear matrix elements (NMEs) and other important aspects, such as quenching. Section 4 outlines the design criteria that must be considered in a $0\nu\beta\beta$-decay experiment. Section 5 presents the broad range of detector technologies, as well as the experimental status and prospects. Section 6 is a summary.

2. PARTICLE PHYSICS ASPECTS

2.1. Why Look for Lepton-Number Violation?

As we emphasize in the introduction, the searches for $0\nu\beta\beta$ decay are searches for lepton-number violation. The lepton number is an accidental global symmetry in the SM. Theories beyond the SM typically violate lepton number unless its conservation is forced by the introduction of additional symmetries.

Lepton-number violation is most often introduced via a $\Delta L = 2$ Majorana mass term for standard or new neutrinos. Grand Unified Theories (GUTs) normally require new neutral fermions; for instance, the 16-dimensional spinorial representation of $SO(10)$ contains all SM particles of a generation plus a right-handed neutrino. Those particles are strongly motivated by the observation of neutrino mass. Left–right symmetric theories or models that gauge the difference of the baryon and lepton numbers, $B - L$, also include right-handed neutrinos with Majorana masses, at least in their minimal formulations. Once the right-handed neutrinos are present, the gauge symmetry of the SM necessarily implies the existence of light massive Majorana neutrinos as a consequence of the seesaw mechanism. An example without any right-handed neutrinos is provided by R-parity-violating supersymmetry, which contains $\Delta L = 1$ terms $\lambda' \ell Q D^c$ that

couple the lepton doublet ℓ, the quark doublet Q, and the down quark singlet D superfields in the Lagrangian. The Majorana neutrino masses are generated at the loop level with two such vertices.

Hence, the arguments for lepton-number violation are strong and plentiful. Its strength, however, is model dependent and needs to be probed experimentally, just as in the searches for baryon-number violation in proton decay and neutron–antineutron oscillation experiments. A well-motivated framework often specifies the scales that need to be tested, such as the nonzero minimal effective mass in the inverted mass ordering of light neutrinos. A typical framework with lepton-number violation would predict not only, within a more or less definite range, the particular $0\nu\beta\beta$-decay half-lives but also other observable quantities. Examples of such quantities include the sum of the neutrino masses (as testable in cosmology) within the standard light-neutrino paradigm, or the cross sections for $eejj$ (same-sign dielectron plus dijet) signals in the heavy-particle exchange scenarios at the Large Hadron Collider (LHC). These predictions allow for experimental checks and the differentiation of individual mechanisms.

The simple observation that there is matter in the Universe implies that some mechanism beyond the SM must exist to create matter. $0\nu\beta\beta$ decay is obviously a process that creates matter, and its observation is crucial for demonstrating ideas about baryogenesis.

It is interesting to consider the energy scales of the physics that could be probed by lepton-number violation and proton decay. In the standard light-neutrino mechanism, the $0\nu\beta\beta$-decay half-life is proportional to Λ^2, where Λ is the scale of neutrino mass generation, for example, the heavy-neutrino mass in the seesaw mechanism. If heavy physics is responsible for the decay, its half-life would be proportional to Λ^{10} with Λ being the mass of the heavy particles. By contrast, proton decay has half-lives that are proportional to the GUT scale Λ in the form of Λ^4 and Λ^5 for nonsupersymmetric (non-SUSY) and SUSY decay modes, respectively. These are obviously very different scales to be tested, and it is difficult to generalize them in model-independent statements.

2.2. Neutrino Mass and Neutrinoless Double-Beta Decay

The observation of neutrino oscillations demonstrated that neutrinos have mass. The two main consequences from the impressive experimental progress in the last two decades are that (*a*) the two different mass-squared differences imply that all neutrino masses are different, with at least two of them being nonzero, and (*b*) lepton mixing is large.

The scalar and fermion content of the SM does not allow for neutrino masses; hence, neutrino oscillations imply physics beyond the SM. It is highly nontrivial to explain this so-called New Physics within a simple paradigm. In this three-Majorana-neutrino paradigm, all phenomena related to neutrino physics are generated by the neutrino mass matrix $m_\nu = U\,\mathrm{diag}(m_1, m_2, m_3)\,U^T$, where m_i are the real and positive neutrino masses and U is the Pontecorvo–Maki–Nakagawa–Sakata (PMNS) matrix containing three mixing angles and three *CP* phases (one Dirac and two Majorana phases).

It is important to note that the smallest neutrino mass is not currently known and that two options for neutrino mass ordering exist: $m_3 > m_2 > m_1$ (normal ordering) and $m_2 > m_1 > m_3$ (inverted ordering). The cases in which the lightest neutrino mass is much smaller than the heavier masses are denoted the normal or inverted hierarchy.

There are altogether nine physical parameters in m_ν, seven of which appear in the effective mass:[1]

$$\langle m_{\beta\beta}\rangle = \left|U_{ei}^2\, m_i\right|. \qquad 3.$$

[1]Only the least-known oscillation parameters, θ_{23} and δ, do not appear.

All seven, except for the two Majorana phases α and β, can be determined by other means—the absolute values of U from neutrino oscillations and the neutrino mass scale from direct kinematic searches or cosmology. We note that this formula holds in the three-Majorana-neutrino paradigm, in which all neutrino phenomenology is determined by three Majorana neutrinos.

In the light-neutrino exchange model, which has hitherto been the most espoused in the physics community, the $0\nu\beta\beta$-decay half-life is

$$T^{0\nu}_{1/2} = \left(G\,|\mathcal{M}|^2\,\langle m_{\beta\beta}\rangle^2\right)^{-1} \simeq 10^{27-28}\left(\frac{0.01\ \text{eV}}{\langle m_{\beta\beta}\rangle}\right)^2 \text{years}. \qquad 4.$$

In this interpretation of $0\nu\beta\beta$ decay, it is a neutrino mass experiment under the assumption that no other mechanism contributes to lepton-number violation and that the neutrinos are Majorana particles.

In Equation 4, the phase-space factor $G \propto Q^5_{\beta\beta}$ is of the order of 10^{-25} (year·eV^2)$^{-1}$ (17, 18). For the NME, $\mathcal{M}$, the approximation $|\mathcal{M}|^2 \sim 10$ is used. From the experimental discussion in Section 5, below, it is clear that tonne-scale experiments are needed to probe the physically interesting regime of $T^{0\nu}_{1/2} \sim 10^{28}$ years and $\langle m_{\beta\beta}\rangle \sim 0.01$ eV. The current limits on $\langle m_{\beta\beta}\rangle$ are approximately 0.2 eV.

For the SM V–A weak interaction, it is worth noting that any observable connected to the Majorana nature of the neutrinos is suppressed by the square of the neutrino mass divided by the energy scale of the process (19). This is why $T^{0\nu}_{1/2}$ is so large compared with that in the $2\nu\beta\beta$-decay process.

The neutrino mass can also be probed by direct kinematic searches, such as the KATRIN (20) and ECHo (21) experiments, as well as by cosmological observations (22). The kinematic searches and cosmological observations are sensitive to

$$m_\beta = \sqrt{|U_{ei}|^2\, m_i^2} \ \text{ and } \ \Sigma = m_1 + m_2 + m_3, \qquad 5.$$

respectively. While the direct kinematic searches provide the most model-independent approach to test the neutrino mass, they give the weakest limits; the projected m_β sensitivity in the KATRIN experiment is 0.2 eV.

Cosmology provides the strongest mass limits in the sum of the neutrino masses Σ. But they depend on the data sets that need to be combined in order to break the degeneracies of the many cosmological parameters. The limits also become weaker when one departs from the seven-parameter framework of ΛCDM (Lambda cold dark matter model) plus neutrino mass (denoted ΛCDM+m_ν) to frameworks with more cosmological parameters. The neutrino mass limits in exotic models of modified gravity are difficult to quantify, but are expected to be weaker as well. The current conservative limits on Σ are approximately 0.3 eV. The readers are referred to the latest Planck data release (23) for a detailed analysis of the cosmic microwave background and other related data. It is noteworthy that a neutrino mass signal is quite likely in future observations within the ΛCDM+m_ν framework, as well as in other moderate extensions, especially if the Planck data are combined with the future Euclid and Square Kilometer Array data (24, 25). This exciting prospect distinguishes the cosmological observations from other approaches.[2] Nevertheless, we repeat that the limits and constraints are hard to quantify in exotic modifications of the minimal ΛCDM+m_ν model; the combination of different data sets is prone to misinterpretations when a multitude of systematic effects are present.

[2]The Project-8 experiment has the ambitious goal of probing m_β to 40 meV, which would cover the inverted-ordering region (26).

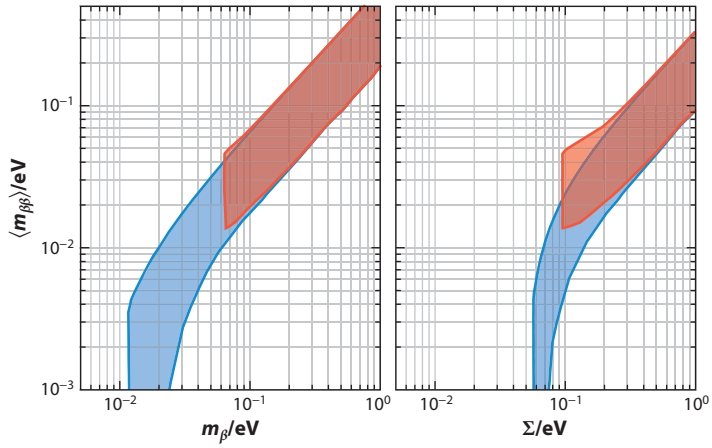

Figure 1

The effective mass $\langle m_{\beta\beta}\rangle$ versus the kinematic neutrino mass observable m_β, and the cosmological observable Σ. The neutrino oscillation parameters are varied within their 3σ ranges. The blue (red) area is for the normal (inverted) mass ordering.

The smallest neutrino mass and the Majorana phases are not known. Varying them allows us to plot the three mass observables against each other, which illustrates nicely the complementarity of the different neutrino mass probes in **Figure 1**. In the scenario of normal mass ordering with hierarchical masses, $\langle m_{\beta\beta}\rangle$ is of the order of meV and can even vanish. In the inverted-ordering scenario, there is a minimum value of approximately 0.013 eV (27). This value represents a physics goal for the current and upcoming $0\nu\beta\beta$-decay experiments.

The current global fits of neutrino oscillation data favor the normal mass ordering over the inverted one by more than 3σ (28). Small tensions in the values of the oscillation parameters Δm^2_{31} and θ_{13} obtained from the long-baseline and reactor experiments contribute to this preference, as does an excess of upward-going electron-like events in the Super-Kamiokande atmospheric neutrino data. The current situation may change; nevertheless, this preference has slowly strengthened with time, as one would expect if it is indeed correct. Note that normal ordering alone does not presuppose a tiny effective mass; the smallest neutrino mass can still be sizable, as normal ordering does not necessitate normal hierarchy.

Bayesian inference can be exploited to quantify the preference for mass ordering by considering the cosmological and neutrino oscillation constraints imposed on the available data (29, 30). The results depend strongly on the choices of the prior (linear or logarithmic) and the parameter space (neutrino masses, or the smallest mass and mass-squared differences, or Σ and mass-squared differences, etc.). Normal ordering is most strongly preferred when the sampling is performed for the three neutrino masses with logarithmic priors (31).

Insights can be gained by using oscillation and cosmology data to obtain the probability distribution for $\langle m_{\beta\beta}\rangle$, from which the discovery potential of future experiments can be inferred (32–34). **Figure 2** shows the Bayesian discovery probability, which corresponds to the chance of measuring a signal with a significance greater than or equal to 3σ. The bands are due to different assumptions in the NMEs. One can draw optimistic conclusions from these Bayesian studies. There is a better-than-50% discovery probability for normal ordering and almost unity for inverted ordering for some of the future experiments.

Beyond SM neutrino physics, the presence of light sterile neutrinos—prompted by LSND, MiniBooNE, short-baseline experiments, and other anomalies—can change the picture

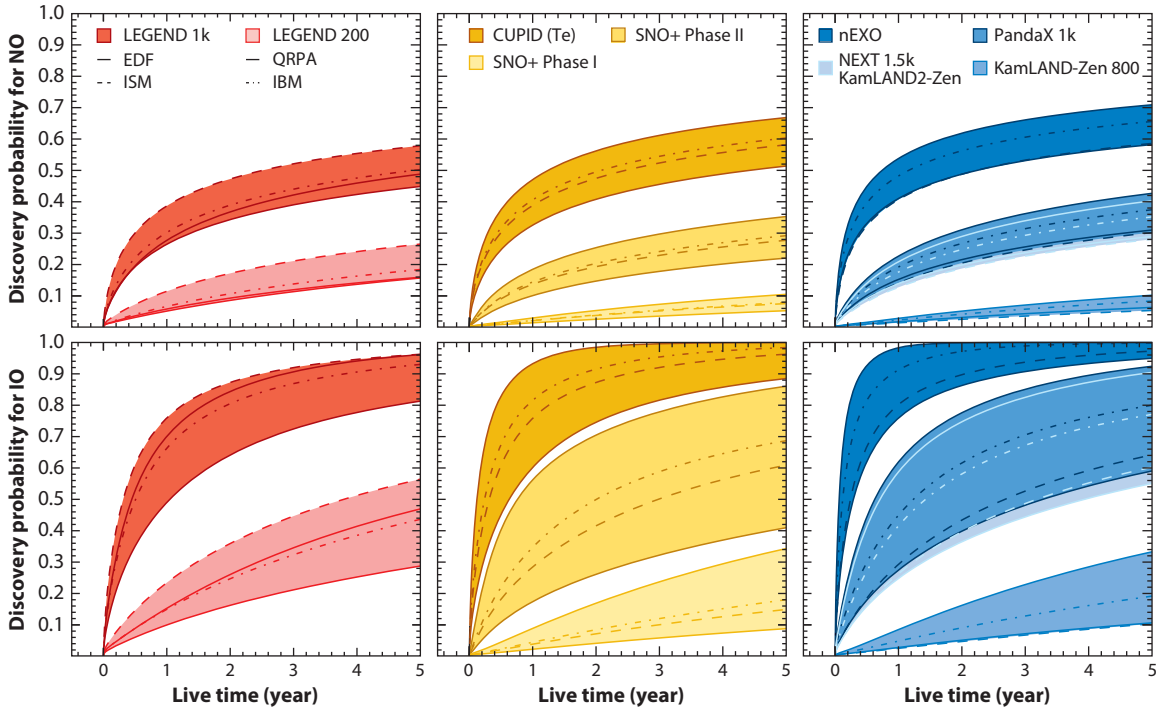

Figure 2

Bayesian discovery probability for future experimental programs (CUPID, KamLAND-Zen, LEGEND, nEXO, NEXT, PandaX, SNO+) as function of running time. The upper (lower) plots are for the normal (inverted) ordering. Abbreviations: EDF, energy-density functional; IBM, interacting boson model; ISM, interacting shell model; QRPA, quasi-particle random-phase approximation. Figure adapted from Reference 33.

dramatically. The additional contribution to the effective mass from sterile neutrinos, $|U_{e4}|^2\, m_4 \simeq |U_{e4}|^2 \sqrt{\Delta m^2_{41}}$, is of the same order of magnitude as the minimal value of the effective mass in the inverted ordering of active neutrinos. It shifts the half-life distribution toward lower values (34); for normal ordering, the shift is toward larger values. The current situation on light sterile neutrinos is confusing (35); most likely, not all hints are correct. Interestingly, the additional sterile-neutrino parameters that enter the effective mass are the same ones that could be responsible for the hints of active-to-sterile oscillation in reactor antineutrinos, for which extensive experimental efforts are being committed. The readers are referred to Reference 36 for a comprehensive review on sterile neutrinos.

2.3. Alternative Mechanisms for Neutrinoless Double-Beta Decay

In the light-neutrino mechanism discussed so far, $0\nu\beta\beta$-decay searches are directly testing light physics. Most alternative mechanisms are short-range mechanisms.[3] If the light neutrino were replaced by a heavy neutrino (i.e., with a mass M_ν larger than the $0\nu\beta\beta$ scale of $|q| = 100$ MeV), the propagator would become

$$\frac{M_\nu}{M_\nu^2 - q^2} \simeq \frac{1}{M_\nu} \ll \frac{1}{\sqrt{|q^2|}}\,. \qquad 6.$$

[3] See Reference 37 for a recent discussion of alternative long-range mechanisms.

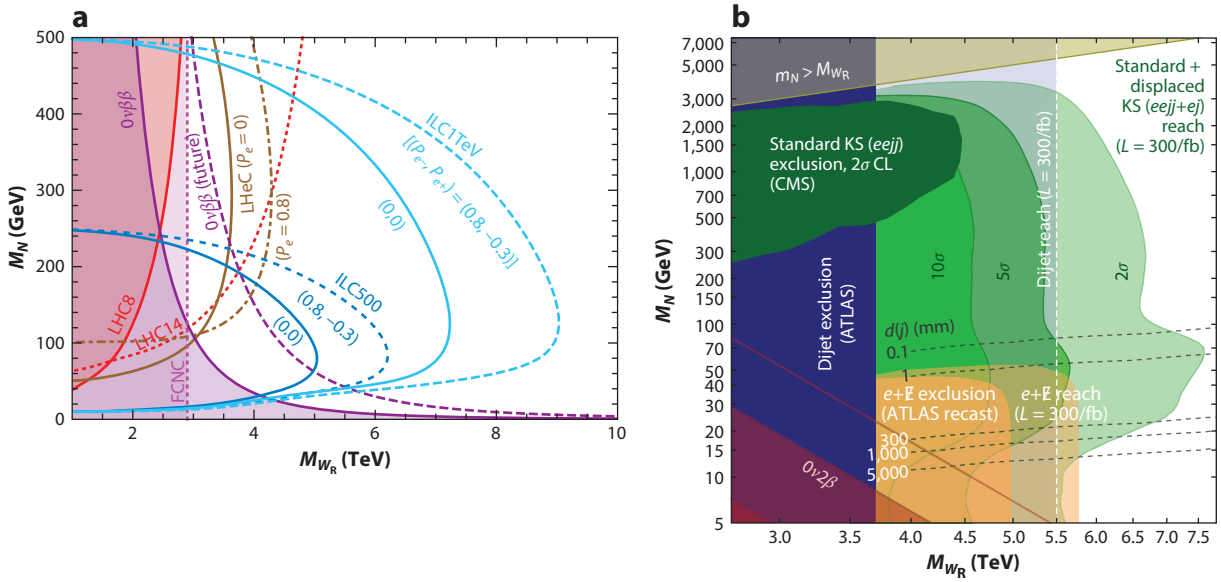

Figure 3

Several examples of constraining and testing alternative $0\nu\beta\beta$-decay mechanisms. (*a*) A comparison between various projected limits from future collider experiments on the right-handed neutrino and gauge boson mass. (*b*) The effects of displaced-vertex analysis on the same parameters. Abbreviations: FCNC, flavor-changing neutral current; ILC, International Linear Collider; KS, Keung–Senjanović; LHC, Large Hadron Collider; LHeC, Large Hadron Electron Collider. Panel *a* adapted from Reference 43. Panel *b* adapted from Reference 41.

In fact, if only heavy particles mediate the decay, the amplitude of the process would be $\mathcal{A}_{\text{heavy}} \sim c/M^5 = (\tilde{c}/M)^5$, where the mass scale M^5 is generally a combination of different particle masses. The corresponding amplitude for the standard one is $\mathcal{A}_{\text{st}} \sim G_F^2 \langle m_{\beta\beta} \rangle / q^2$. The current limit of $\langle m_{\beta\beta} \rangle$ yields $\mathcal{A}_{\text{st}} \sim (0.3\,\text{TeV})^{-5}$, demonstrating that lepton-number-violating TeV-scale physics would generate $0\nu\beta\beta$-decay half-lives corresponding to the current limits. This simple but illustrative and reasonably accurate estimate is the basis of many works on testing alternative $0\nu\beta\beta$-decay diagrams with the same-sign dilepton processes (38) $pp \to eejj$ at the LHC, or similar processes at other colliders.

By modifying Equation 4, we can express the half-life for heavy physics mechanisms very approximately (i.e., with much wider spread than the light-neutrino expression) as

$$T_{1/2}^{\text{heavy}} \sim 10^{27-28} \left(\frac{\tilde{c}/M}{\text{TeV}} \right)^{10} \text{years}. \qquad 7.$$

A typical LHC test would work via the resonant production of a vector boson, and a Majorana fermion causes the subsequent lepton-number violation. The new particles in the $0\nu\beta\beta$-decay diagram are not required to have the same or similar mass. The fermion could be much lighter than the vector boson, in which case the leptons and jets would be of low energy and would escape detection in the analysis. Displaced-vertex searches, such as those shown in **Figure 3**, are helpful in such instances (39–41). Future e^+e^- or ep colliders have different characteristics in particle kinematics, allowing experiments to probe different areas in the parameter space. Moreover, the polarization of the initial-state fermions can help disentangle the chiral nature of the underlying process (42, 43). Recent reviews on the tests of neutrino mass models and lepton-number violation at colliders can be found elsewhere (44, 45).

As an example, there are left–right symmetric theories that contain heavy right-handed neutrinos N_R and gauge bosons W_R with mass M_{W_R}. Several diagrams for $0\nu\beta\beta$ decay arise in those theories (46–48), for instance, purely right-handed ones with N_R and W_R exchange, or mixed diagrams with light-neutrino exchange in which one of the currents is right-handed. The electrons in the latter diagrams are emitted with different helicities, which affect their angular distribution. The energy distribution of the individual electrons is also different, which in principle would allow the driving mechanisms to be distinguished if the electrons can be tracked. Such an analysis has been performed in the SuperNEMO project (49).

A natural question to ask is whether $0\nu\beta\beta$ decay or collider limits will provide better constraints on the relevant model parameters. The answer depends on the various corrections that have not been studied for all mechanisms. As an example, a model with a $Y = 1$ $SU(2)_L$ doublet scalar and a singlet fermion was discussed in References 50 and 51. With various experimental and theoretical corrections included, it was shown (51) that $0\nu\beta\beta$ decay would provide better reach in the search for TeV-scale lepton-number-violating interactions. The size of many theoretical corrections, however, is not completely understood and is a subject of debate. Nevertheless, LHC and $0\nu\beta\beta$-decay searches are complementary approaches that provide a consistency check in case of a discovery.

Lepton-number violation observed at TeV scale has interesting cosmological implications. It is possible to translate an observed cross section of a lepton-number-violating process at the LHC into lepton-number-violating washout processes in the early Universe (52, 53). Any lepton asymmetry generated by standard high-scale leptogenesis would typically be washed out, making this baryogenesis mechanism ineffective. With TeV-scale lepton-number violation, there is not really a need for standard high-scale leptogenesis; nevertheless, the interesting consequences of a TeV-scale observation of a $0\nu\beta\beta$-like process are obvious.

The black box, or Schechter–Valle, theorem (7) states that any diagram causing $0\nu\beta\beta$ decay will generate a Majorana mass term for light neutrinos, rendering them Majorana particles. However, this is generally a mass term generated by a four-loop diagram that leads to a minuscule mass (54) of the order of $\epsilon/(8\pi^2)^4 G_F^2 m_q^6/m_p \lesssim 10^{-29}$ eV, where we have used $m_q = 5$ MeV and $\epsilon \lesssim 10^{-7}$ (see next paragraph). In certain models, the connection of the $0\nu\beta\beta$ operator to a Majorana mass may be more direct. Examples are diagrams in which the particles that generate $0\nu\beta\beta$ decay are the same ones that generate the neutrino mass in one-loop mechanisms.

One can write a general Lagrangian responsible for $0\nu\beta\beta$ decay via short-range mechanisms (55):

$$\mathcal{L}_{\text{short}} = \frac{G_F^2}{2m_p}\left\{\epsilon_1^X JJj + \epsilon_2^X J^{\mu\nu}J_{\mu\nu}j + \epsilon_3^X J^\mu J_\mu j + \epsilon_4^X J^\mu J_{\mu\nu}j^\nu + \epsilon_5^X J^\mu J j_\mu\right\}, \qquad 8.$$

where $J = \bar{u}(1 \pm \gamma_5)d$, $j = \bar{e}(1 \pm \gamma_5)e^c$, $J_{\mu\nu} = \bar{u}(i/2)[\gamma_\mu, \gamma_\nu](1 \pm \gamma_5)d$, $J_\mu = \bar{u}\gamma_\mu(1 \pm \gamma_5)d$, and $j_\mu = \bar{e}\gamma_\mu(1 \pm \gamma_5)e^c$. The chirality of the operators is encoded in $X = abc$, where a, b, or c is L or R. If some heavy physics generates lepton-number violation at a scale Λ, one can generate effective operators as in Equation 8, where ϵ decreases with Λ. The product of three fermion currents illustrates that $0\nu\beta\beta$ decay in the short-range scenario can be described by dimension-nine operators. While there are 24 independent operators (56), only a few of them appear in nonexotic theories beyond the SM. The limits on the various ϵ^X are around 10^{-7} to 10^{-10} (56, 57). An example within a well-known extension of the SM is a diagram with heavy right-handed bosons W_R and right-handed neutrinos mediating the decay. In this case, $\epsilon_3^{RR} = V_{ei}^2 m_p (m_W/M_{W_R})^4/M_i$, where V is the right-handed lepton mixing matrix and M_i is the masses of the heavy neutrinos.

Finally, we note that several mechanisms for $0\nu\beta\beta$ decay may be present at the same time. They could even interfere with one another (58) as long as the helicities of the emitted electrons allow for that.

2.4. QCD Corrections

QCD corrections to $0\nu\beta\beta$-decay diagrams are important (48, 51, 59–63). Naïvely, the effect is of order $\alpha_s/(16\pi^2)\log\Lambda^2/q^2 \simeq 0.1$, where Λ is the scale of the mechanism and $q^2 \simeq (100\,\mathrm{MeV})^2$ is the scale of the nuclear process. However, a Fierz transformation might be needed to generate a color-singlet final state that can be sandwiched between final-state nucleons. This procedure generates operators with different Lorentz structures, which can have drastically different NMEs, and so generates sizable corrections. The standard light-neutrino exchange diagram does not generate additional operators after applying the Fierz transformation to the QCD-corrected one; thus, it is not significantly affected by QCD corrections. Applying QCD corrections (as electroweak corrections are much smaller) (51, 59, 60), the operators in Equation 8 are supposed to be run down to the scale of $0\nu\beta\beta$ decay of approximately 100 MeV. Below 1 GeV, the strong coupling becomes too large for applying perturbative techniques. There are ideas to cover this regime, but their numerical impact is not yet clear. QCD corrections to the long-range mechanisms are expected to be smaller than the NME uncertainties (64).

2.5. Alternative Processes

Over the years, there have been suggestions of other processes to probe low-energy lepton-number violation, to identify the neutrino mass nature, or to entail both (see Reference 19 for a recent summary). The observation of these modes typically requires either nonrelativistic neutrinos (65–69) or new interactions (70, 71). For heavier neutrinos, the effects are observable only in certain mass ranges, such as in meson or W decays (72).

Neutrinoless double-electron capture (73), $(A, Z) + 2e^- \rightarrow (A, Z-2)$, was of interest as an attractive alternative to $0\nu\beta\beta$ decay, since there was the possibility of a resonant enhancement if the initial- and final-state energies are close to degenerate (74). However, precise measurements of the involved nuclear masses disfavor this option (75, 76). In addition, the decay to excited states, neutrinoless double-positron decay, or various combinations of electron capture and β or positron decay suffer from very low rates. Their observation would be a consistency check of the underlying mechanism of lepton-number violation and could provide useful information about the nuclear physics in neutrino-accompanied processes. $0\nu\beta\beta$ remains the most optimistic channel to answer the pressing questions of lepton-number violation and the neutrino nature.

3. NUCLEAR AND HADRONIC PHYSICS ASPECTS

The NME for $0\nu\beta\beta$ decay can be written formally as

$$\langle \mathrm{final}|\mathcal{L}_{\ell-N}|\mathrm{initial}\rangle. \qquad 9.$$

What is needed for its evaluation are nuclear structure calculations for the final and initial nuclear states, as well as a proper transition from the fundamental lepton–quark Lagrangian to the lepton–nucleon one, $\mathcal{L}_{\ell-N}$. Both problems are essentially independent of each other. Determining the accuracy and uncertainties of the various possible NMEs can be considered the most challenging theoretical problem that hinders precision studies of $0\nu\beta\beta$ decay in the event of a discovery.

3.1. Hadronization

While the fundamental $0\nu\beta\beta$-decay Lagrangian is written at the quark level, hadrons are present in the nucleus. Moreover, operators need to be run from the fundamental high-lepton-number-violating scale down to the nuclear scale, and then matched to the operators built from the

hadronic degrees of freedom. A problem is that the hadronic operators are often phenomenologically written in terms of the form factors when the transition between quarks and nucleons is made, as in $\langle p|\bar{u}(1-\gamma_5)d|n\rangle = e^{-i(p-p')x}\bar{u}(p)(F_S(q^2)+F_{PS}(q^2)\gamma_5)u(p') \equiv J_{S-P}$. In this example, $u(p)$ and $u(p')$ are the spinors for the initial- and final-state neutron, and $p'-p=q$. The q^2 dependence of several form factors (particularly for scalar and pseudoscalar) is unknown, as is their normalization (particularly for tensor). The induced currents are also important, as one can see by considering the following nucleon matrix element that is particularly relevant for light-neutrino exchange:

$$\begin{aligned}\langle p|\bar{u}\gamma^\mu(1-\gamma_5)d|n\rangle \equiv J^\mu_{V-A}(x) = \bar{u}(p)\big(F_V(q^2)\gamma^\mu - iF_W(q^2)/(2m_p)\sigma^{\mu\nu}q_\nu \\ - F_A\gamma^\mu\gamma_5 + F_P(q^2)/(2m_p)\gamma_5 q_\mu\big)\,u(p')e^{iqx}\,. \qquad 10.\end{aligned}$$

The normalization factors $F_i(q^2=0)$ are the coupling constants; $F_V(q^2=0)=g_V$ and $F_A(q^2=0)=g_A$ are the vector and axial-vector coupling constants.

One can use the language of chiral symmetry (48, 51, 63, 77, 78) and effective field theory (79) to identify the necessary (i.e., the ones with the same symmetry structure under chiral symmetry) and leading hadronic operators. In chiral power counting, the $\pi\pi\,ee$ operator is the leading one, corresponding to a pseudoscalar interaction (two neutrons exchange a pion, which converts from a π^- to a π^+). There is an ongoing effort from the lattice QCD community to provide pion-level NMEs and the necessary low-energy coupling constants of the operators (80–82). In general, pion exchange implies a long-range interaction, which overcomes the usual suppression of the short-range diagrams. In mechanisms that induce pseudoscalar operators at the tree level, such as R-parity-violating SUSY, pion exchange can be expected to dominate (83, 84). A general effective field theory framework that connects a chain of effective field theories through various scales, including those at lepton-number violation, electroweak-symmetry breaking, chiral-symmetry breaking, and m_π, has recently been formulated (48).

The induced pseudoscalar current that is proportional to F_P in Equation 10 is also connected to pion exchange. It has been argued (84) that the correction to the leading Gamow–Teller matrix element is of the order $q^2/(q^2+m_\pi^2)\sim 30\%$ in the light-neutrino case. Recently, References 85 and 86 revisited the short-range contributions to the light-neutrino mechanism by using the chiral language mentioned above. Diagrams with $\pi\pi\,ee$ couplings generate ultraviolet divergences in the $nn\to pp\,ee$ amplitude, which can be cured by a counterterm in the form of a nucleon–nucleon contact term. Recent lattice calculations also identified a possibly important short-distance contribution (81). While leading in chiral power counting, its size is currently not determined well, and its impact is not clear.

3.2. General Aspects of the Nuclear Matrix Elements

Focusing on the most-referenced light-neutrino mechanism, we consider the quark-level current $J^\mu = \bar{u}\gamma^\mu(1-\gamma_5)d$. As a second-order process, a time-ordered integration is needed:

$$\int d^4x\,d^4y\,\langle f|T\{J^\mu(x)J^\nu(y)\}|i\rangle \propto \sum_n \frac{\langle f|J^\mu(\vec{q})|n\rangle\,\langle n|J^\nu(-\vec{q})|i\rangle}{|\vec{q}|(E_n+|\vec{q}|+E_{e2}-E_i)} + (e2\to e1, \mu\leftrightarrow\nu), \qquad 11.$$

which implies the introduction of a complete set of intermediate states of energy E_n. All states up to approximately 100 MeV contribute.[4] The impulse approximation for the nuclear current J^μ_{V-A}

[4]In contrast, the SM-allowed $2\nu\beta\beta$ decay has only 1^+ intermediate states (as two real neutrinos are emitted) with energies up to $Q_{\beta\beta}$ of a few MeV.

in Equation 10 sums over the individual free-nucleon matrix elements; in other words, only one nucleon experiences the weak decay without interference from the surrounding nuclear medium. The form factors (see Section 3.1) need to be properly expanded in a nonrelativistic form. Various other approximations would then lead to the general formula in Equation 4.

The NME is

$$\mathcal{M} = \mathcal{M}_{\mathrm{GT}} - \frac{g_V^2}{g_A^2}\mathcal{M}_{\mathrm{F}} + \mathcal{M}_{\mathrm{T}}, \qquad 12.$$

where the Fermi matrix element $\mathcal{M}_{\mathrm{F}}$ depends on the integral over $|\vec{q}|$ of $F_V(\vec{q}^{\,2})$ in its nonrelativistic approximation, whereas the Gamow–Teller matrix element $\mathcal{M}_{\mathrm{GT}}$ depends on the corresponding integrals over linear combinations of $F_{A,P,W}(\vec{q}^{\,2})$ (see References 56 and 87 for the explicit expressions). The tensor matrix element $\mathcal{M}_{\mathrm{T}}$ can be neglected. As an example, the Gamow–Teller matrix element, which is the leading one, can be written as

$$\mathcal{M}_{\mathrm{GT}} = g_A^2 \frac{2R}{\pi} \int_0^\infty d|\vec{q}|\,|\vec{q}|\langle f| \sum_{a,b} \frac{j_0(|\vec{q}|r_{ab})\, h_{\mathrm{GT}}(|\vec{q}|\vec{\sigma}_a \cdot \vec{\sigma}_b)}{|\vec{q}| + \bar{E} - (E_i + E_f)/2} \tau_a^+ \tau_b^+ |i\rangle, \qquad 13.$$

where R is the nuclear radius of $1.2A^3$ fm, j_0 is the Bessel function, h_{GT} is a combination of $F_{A,P,W}$ properly expanded, and $\vec{r}_{ab}$ is the distance between the two decaying nucleons. Short-range correlations may be important, particularly for short-range mechanisms. The repulsion at short distances can be phenomenologically described by the UCOM, Jastrow, Argonne, or Bonn potential, with which the operators in the NMEs are multiplied.

The difficulty of NME calculations is to know the initial- and final-state nuclear wave functions, a many-body problem that in practice allows no exact solution. Several approaches to the problem exist and have been summarized in recent reviews (87–89). **Figure 4** depicts the status

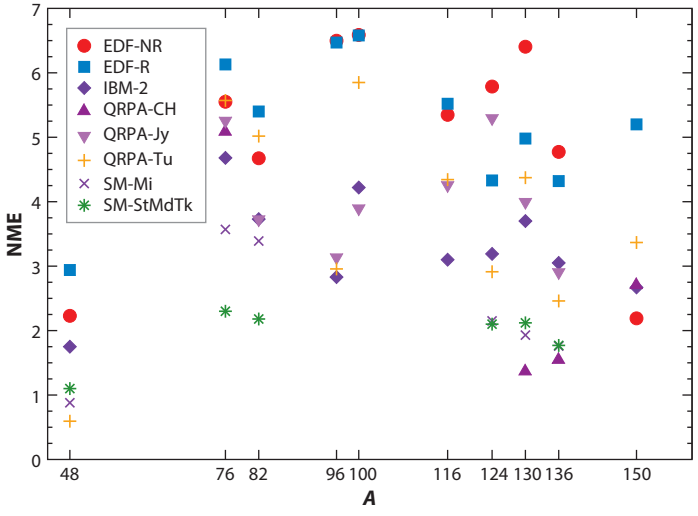

Figure 4

A representative compilation of nuclear matrix element calculations with an unquenched $g_A = 1.27$ for different isotopes (see Reference 87, and references therein, for details). Abbreviations: EDF, energy-density functional; IBM, interacting boson model; NME, nuclear matrix element; QRPA, quasi-particle random-phase approximation; SM, Standard Model.

of NME calculations for the different approaches. We summarize the main approaches in the remainder of this section.

The energy-density functional (EDF) and the generator coordinate methods (GCM) mix many mean fields with different properties (90–92), whereas the other methods use simple mean fields that the states and orbitals feel. Minimization of the energy functional finds the ground states. A large number of single-particle states are included and their collective motion is treated, but only a few selected correlations are used, possibly leading to an overestimation of the NME. The Projected Hartree–Fock–Bogoliubov Method (PHFB) is a related approach (93).

The nuclear shell model (NSM) does not use the full Hilbert space of the nucleon states, but only those in a valence space near the Fermi surface (94, 95). The limited number of active nucleons and oscillator shells means that the low-lying states can be well described and reproduced, although the effects of pairing correlations may not be fully captured and may lead to an underestimation of the NME. Indeed, enlarging the configuration space would increase the matrix elements (96).

The interacting boson model (IBM) features nucleon pairs represented as bosons with certain quantum numbers and features a truncation of the full shell-model space to a subspace. More shells are used than in the NSM, but with fewer correlations (97–99). The description is typically more phenomenological than the other methods, and relies more on adjusting the model parameters to match the observables.

The quasi-particle random-phase approximation (QRPA) contains few correlations but a large number of single-particle orbits (100–102). The proton–neutron interaction quantified by a parameter g_{pp} should equal one in an exact calculation and diagonalization; it is fixed to a value that reproduces the measured $2\nu\beta\beta$-decay half-lives. Also, the particle–hole coupling parameter can be fixed by observables.

The ab initio methods are a recent and promising line of development. All nucleons are taken as degrees of freedom, and interactions are fitted from the data involving nucleons or small nucleon systems. These approaches are currently limited by the availability of computing power. However, the recent results within the NSM for light isotopes (103) and the $0\nu\beta\beta$-decay candidate ^{48}Ca are encouraging (104).

All approaches miss certain features. Naïvely, one expects that the lack of configurations underestimates the NME, while the lack of correlations overestimates them, which is what the distribution in **Figure 4** seems to confirm. There is hope that the calculations will converge as their respective shortcomings are overcome by future improvements. We refer readers to the authoritative nuclear physics review in Reference 87, which discusses those attempts in detail.

The uncertainties in the NMEs are difficult to quantify. Some effects would shift all matrix elements, for example, the possible quenching of g_A (see Section 3.3), while others are only applicable to certain models, such as the particle–particle coupling within QRPA. Although it is possible to study the effects by varying the nuclear model parameters (105), it is less clear how to quantify the shortcomings of the models in a systematic way. These desperately needed studies are under way as the associated uncertainties are expected to be larger than those from varying the model parameters. A multi-isotope $0\nu\beta\beta$-decay program would surely help quantify and understand the current discrepancies.

3.3. Quenching

With the Gamow–Teller matrix element $\mathcal{M}_{\mathrm{GT}}$ the leading one in the light-neutrino exchange case, the NME is to a good approximation proportional to g_A^2, and $T_{1/2}^{0\nu}$ is proportional to g_A^{-4}. Quenching denotes the reduction of g_A that is necessary to reproduce the observable quantities of

nuclear decays (106), particularly β and $2\nu\beta\beta$ decays (see Reference 107 for a review). In addition, low-energy forward-angle charge-exchange reaction tests of the Ikeda sum rule confirm a reduced Gamow–Teller strength (108), as do the spectral measurements of forbidden β decays (109). A reduced g_A implies a longer $T^{0\nu}_{1/2}$, which is undesirable for experimental searches (98, 99, 110). Other alternative $0\nu\beta\beta$-decay mechanisms would also be affected by quenching, though possibly to a lesser extent as $\mathcal{M}_{GT}$ may not be the leading element.

The value of g_A is used as an adjustment to bring observations in agreement with calculations. When the strength of the Gamow–Teller operator needs to be reduced, one reduces the axial coupling constant from its free nucleon value of 1.27. Possible origins of quenching are nuclear-medium effects, many-body currents, or the inherent shortcomings of the nuclear many-body models. A possibly important observation is that β and $2\nu\beta\beta$ decays have energy scales of order MeV, that is, much smaller than the $0\nu\beta\beta$ scale of order 100 MeV. Low-energy processes may require more quenching as the missing particle–hole excitations in the models may shift the Gamow–Teller strength to higher energies. Thus, less or no quenching might be needed in $0\nu\beta\beta$ decay. However, conflicting statements in the literature exist. The dependence of quenching on the nuclear calculations can be demonstrated by analyzing the $2\nu\beta\beta$ electron-energy spectra (111), which allows the extraction of the subleading higher-order contributions to the matrix elements (112).

Nonnucleon degrees of freedom or many-nucleon currents may also shed light on the issue (113–115). In β and $2\nu\beta\beta$ decays, long-range pion exchange reduces the matrix elements significantly, whereas a reduction of only 10–30% was observed in $0\nu\beta\beta$ decay (as pion exchange contributes less at higher momenta). There are also indications that muon capture on nuclei requires less quenching, which again implies an energy dependence of the effect.

In summary, recent studies indicate that there is less quenching necessary (not more than 20–30%) in processes with large momentum transfer such as $0\nu\beta\beta$ decays. This reduction would correspond to an increase of $T^{0\nu}_{1/2}$ by a factor of approximately two to three. However, there is not yet consensus in the literature on this issue, and further experimental inputs and improvements in the calculations are desperately needed.

3.4. Experimental Tests of the Nuclear Matrix Elements

Hadronic charge-exchange reactions, whose transition matrix elements[5] (related to the products of two β-decay Gamow–Teller matrix elements) can be accessed through reactions in the β^- and β^+ directions (116), provide a good test for the matrix elements in $2\nu\beta\beta$ decay. The neutrinoless mode and its NME problem can benefit from such nuclear structure measurements. For instance, the determination of the neutron occupancies in (p,t) two-nucleon transfer experiments (117) has significantly influenced the QRPA calculations of the NMEs (118). One is normally interested in the Gamow–Teller operators, and has to choose reactions with small momentum transfer at the forward angles. With the proper choice of kinematics, charge-exchange reactions can also probe the transition strengths to the states beyond 1^+. However, the hadronic operators do not exactly mimic $0\nu\beta\beta$ decay, and the crucial phases of the states are not accessible.

The NUMEN Collaboration (119) recently presented a new approach. The goal is to use heavy-ion-induced double-charge-exchange reactions to test the second-order isospin response. Even at the forward angles, sizable momenta are transferred. Other similarities to $0\nu\beta\beta$ decay

[5]The charge-exchange reactions are mediated by nuclear transitions to the same spin, isospin, and multipole operators. Thus, they can be used as tests of the weak interaction, in particular, as tests of the isospin response.

include complex nuclear medium effects and off-shell intermediate states of the reaction.[6] The first measurements of the ^{40}Ca(^{18}O,^{18}Ne)^{40}Ar reaction were performed (122) to demonstrate the experimental principle. Work is under way to probe reactions that involve the isotopes in $0\nu\beta\beta$-decay searches. Apart from various nuclear structure information, the quenching issue can also be addressed. The latter is also possible in muon-capture reactions (123).

4. EXPERIMENTAL DESIGN CRITERIA

The observables in direct searches of $0\nu\beta\beta$ decay are the kinematic parameters of the two emitted electrons. A typical experiment measures the total energy (E) of the two electrons and may be able to reconstruct the individual electron paths (tracking) to reject backgrounds based on event topology. The observed $0\nu\beta\beta$-decay signal is a monoenergetic peak at $Q_{\beta\beta}$ as there are no antineutrinos emitted in the decay. Since $Q_{\beta\beta}$ is well measured, usually in high-precision atomic traps, the signal search can be performed over a narrow energy window around $Q_{\beta\beta}$; the width of this region of interest (ROI) is selected on the basis of the energy resolution of the detector. The number of candidate events, N, observed in the ROI is

$$N = \ln(2)\frac{N_A}{W}\left(\frac{a\,\varepsilon\,Mt}{T^{0\nu}_{1/2}}\right), \qquad 14.$$

where N_A is Avogadro's number, W is the molar mass of the source, a is the isotopic abundance of the parent isotope, ε is the detection efficiency of the signal in the ROI, and t is the measurement time. The last factor of this expression captures the choices that an experimenter can make in designing an experiment.

The sensitivity to the half-life obviously would depend on the total number of counts in the ROI, some of which may be background events:

$$(T^{0\nu}_{1/2}) \propto \begin{cases} a\,M\,\varepsilon t & \text{background free,} \\ a\varepsilon\sqrt{\dfrac{Mt}{B\,\Delta E}} & \text{with background,} \end{cases} \qquad 15.$$

where ΔE is the detector energy resolution and B is the background index, normalized to the width of the ROI, source mass, and measurement time, for instance, in units of (keV·kg·year)$^{-1}$. This expression clearly shows the advantage of a background-free experiment, as the $T^{0\nu}_{1/2}$ sensitivity would scale linearly with t as opposed to $\sqrt{t}$ in the presence of backgrounds. In the following subsections, we discuss some of the design considerations in a $0\nu\beta\beta$-decay experiment, including the choice of isotopes, sources of backgrounds, and their mitigation and elimination.

4.1. Isotope Choices

There are 35 isotopes capable of $\beta\beta$ decay (125), but not all of them are suitable as candidate isotopes for direct searches of $0\nu\beta\beta$ decays. **Table 1** lists the characteristics of some of the isotopes that have been deployed in experiments. Given Equation 15, an ideal isotope should have a high isotopic abundance (large a) and can be deployed in large quantity (large M) as high-resolution detectors (small ΔE) under low-background conditions (small B). Unfortunately, such an isotope does not exist, and experimenters have to make design choices to optimize a subset of these parameters.

[6]Measurements of the double Gamow–Teller giant resonance are suggested to have a linear correlation to the $0\nu\beta\beta$-decay matrix element (120; see, however, Reference 121).

Table 1 Characteristics of commonly used $\beta\beta$-decay isotopes

Isotope	Natural abundance (%)[a]	$Q_{\beta\beta}$ (MeV)
^{48}Ca	0.187	4.263
^{76}Ge	7.8	2.039
^{82}Se	8.7	2.998
^{96}Zr	2.8	3.348
^{100}Mo	9.8	3.035
^{116}Cd	7.5	2.813
^{130}Te	34.08	2.527
^{136}Xe	8.9	2.459
^{150}Nd	5.6	3.371

[a]The isotopic abundances are obtained from Reference 124.

The most critical consideration is the potential sources of backgrounds. An irreducible background to the $0\nu\beta\beta$-decay search consists of the $2\nu\beta\beta$-decay electrons; they are indistinguishable from those in the $0\nu\beta\beta$-decay mode in the ROI. One way to mitigate this background is to deploy an isotope with a long $2\nu\beta\beta$-decay half-life. The ratio of the $0\nu\beta\beta$-decay signal to the $2\nu\beta\beta$-decay background, S/B, is approximately (14)

$$\frac{S}{B} \propto \left(\frac{Q_{\beta\beta}}{\Delta E}\right)^6 \frac{T_{1/2}^{2\nu}}{T_{1/2}^{0\nu}}, \qquad 16.$$

which indicates the importance of an excellent detector energy resolution for isotopes that have shorter $2\nu\beta\beta$-decay half-lives.

Primordial radioisotopes from the U and Th chains are ubiquitous in the detector construction materials. The most troublesome one is ^{208}Tl. Its 2,615-keV γ-ray line lies above $Q_{\beta\beta}$ for a number of $\beta\beta$-decay isotopes, and can deposit energy extraneously within the ROI. Another problematic background comes from ^{222}Rn, whose progeny ^{214}Bi emits a β electron with an energy up to 3,270 keV. An ideal $0\nu\beta\beta$-decay isotope candidate would have a $Q_{\beta\beta}$ high enough to avoid these backgrounds.

The detection efficiency of the $0\nu\beta\beta$-decay signal can be significantly enhanced if the source material is integrated as the detector medium. As the path lengths of the two signal electrons are much shorter than the size of the active medium in such a coalesced configuration, calorimetry with excellent energy resolution is possible. When the source material is external to the detector, the probability of at least one of the two electrons escaping detection or with degraded energy increases due to self-absorption. The main advantage of this external-source configuration is the possibility of superior tracking and effective background rejection, but at the expense of energy resolution.

To reduce the cost of an experiment, an ideal source material should be readily available in its natural form and the candidate isotope within it should have a high natural abundance. The cost of isotope enrichment typically depends on the isotopic abundance of the starting material—the higher the natural abundance, the lower the cost. If the natural abundance is high enough, isotope enrichment may be unnecessary, as has been demonstrated in the case of ^{130}Te (126). Reference 12 provides a succinct summary of the enrichment of $\beta\beta$-decay isotopes.

4.2. Backgrounds

The $T_{1/2}^{0\nu}$ discovery potential would shrink substantially in the scenario of a nonvanishing background index. For the next generation of experiments to reach a discovery potential of

$T_{1/2}^{0\nu} \sim 10^{28}$ years, an extremely stringent background index of <0.1 count/(FWHM·tonne·year), where FWHM is the full width at half maximum of the detector resolution at $Q_{\beta\beta}$, is necessary. Readers are referred to References 127 and 128 for a comprehensive review of backgrounds in sensitive underground experiments. What follows is a brief introduction.

As discussed above, a careful choice of target isotope and detector technology could diminish the impact of the irreducible $2\nu\beta\beta$-decay background on the discovery potential. Similarly for the omnipresent solar neutrinos, their impact can be mitigated by a high mass loading of the decaying isotope in the target medium to improve the ratio of the signal to the neutrino–electron elastic scattering background. This is particularly important for large (kilotonne-scale) liquid-scintillator detectors.

In $0\nu\beta\beta$-decay experiments, several types of backgrounds can be controlled through careful design and vigilant implementation. Trace amount of radioisotopes from the natural U and Th chains must be kept to a minimum in any materials close to active detector volume. Other pervasive natural radioactivities, such as ^{3}H, ^{14}C, and ^{40}K, have lower decay energies and do not impinge on $0\nu\beta\beta$-decay searches. The techniques to produce radiopure materials for mechanical support are constantly being explored and refined, for example, electroformed Cu and alloys (129, 130) and polymers (131). Radioassay results from prior generations of low-background experiments (132–134) are now readily accessible as online databases (135) to aid the material selection process for future experiments. Even when intrinsically radiopure construction materials have been identified, extreme care to maintain their cleanliness is essential. For example, exposure to ^{222}Rn would result in increased α and β emitter backgrounds on the surface or in the bulk of the unprotected components.

Natural radioactivities far away from the active detector volume, including γ-rays from the primordial chains and neutrons from (α, n) reactions originating from the rock wall of the underground laboratory, can be blocked by passive shielding with clean Pb or Cu, water, or liquid cryogen. The last two options may also allow the shielding medium to serve as an active veto to reject cosmic rays.

Cosmic-ray muons (μ) can induce several types of background in a $0\nu\beta\beta$-decay experiment. For experiments at deep underground laboratories, prompt muon interactions in the detectors do not usually pose any background concerns. These interactions typically deposit a large amount of energy and can be vetoed easily. The activation of long-lived isotopes and the production of secondary neutrons are the main worries. Muons can induce these backgrounds via different mechanisms: μ^- capture in nuclei (136–138), muon–nucleon quasi-elastic scattering, electromagnetic showers, and photo-neutron production through virtual photon exchange. High-energy neutrons produced in inelastic neutron scattering $(n, n'\gamma)$ are also a source of background in $0\nu\beta\beta$-decay experiments (139, 140).

Numerous theoretical and experimental studies have been performed to determine the production yield of these radioisotopes after the materials that are commonly used in dark matter and $\beta\beta$-decay searches have been exposed to cosmic rays at or above the Earth's surface (see, e.g., References 141–144 on target materials and References 145–147 on construction materials). There are two strategies to mitigate these activated backgrounds: to minimize the exposure to cosmic rays on the surface and to let the materials cool down underground after such exposure. However, it would be impractical to wait for certain long-lived radioisotopes to decay to an acceptable activity.

The backgrounds from cosmogenic production of radioisotopes in situ during the experiment are difficult to identify, as their decays could occur long after the initial muons. Although this is an irreducible background, its impacts can be mitigated by simply deploying the experiment at a greater depth. This type of background is of particular concern to experiments in which the

$\beta\beta$-decay isotopes are dissolved in a large volume of host medium [e.g., liquid scintillator (148)] given the large mass and the broad energy spectrum of the activated products. Experiments with tracking or event position reconstruction capabilities can reject these backgrounds by temporal and spatial correlations (e.g., 149).

4.3. Detection Strategies

As with any search for New Physics, the primary goal of the detector design is to discriminate between signal and backgrounds effectively while maintaining high signal detection efficiency. The most common way to achieve this discrimination is via energy resolution, which is generally intrinsic to the detection medium. For the next generation of experiments, it will also be essential to maximize the discovery potential. This means actively showing that any observed signal is not only consistent with the expected $0\nu\beta\beta$-decay signal but also inconsistent with the measured backgrounds. The pitfall of relying on energy alone to make a discovery claim is illustrated by Reference 150.

$0\nu\beta\beta$ has a characteristic event topology with the emission of two ~MeV electrons. Low-density-gas tracking detectors can in principle resolve the two electron tracks, leaving only the irreducible background from $2\nu\beta\beta$ decay. For detectors with higher density, such as discrete detectors or liquid-scintillator detectors, these electrons deposit their energy within a few millimeters, allowing a less powerful but still useful discrimination between compact signal-like events and γ-rays, which are likely to scatter and deposit energy at multiple sites. The difference may be resolved through discriminating between the so-called single-site and multisite events by pulse-shape discrimination or reconstructed event topology, depending on the position resolution, as well as the size and type of a given detector. Some detectors are capable of particle discrimination through multiple detection channels, such as scintillation and ionization, which could allow for the identification of α backgrounds.

Timing is yet another key variable for distinguishing signal from backgrounds. For example, in the aforementioned ^{222}Rn chain, the particularly troublesome ^{214}Bi progeny decays in coincidence with ^{214}Po α decay, which has a 160-μs half-life. For some detectors, this timing coincidence can be used to identify ^{214}Bi decays both in the bulk material and on the surfaces.

The spatial distribution of background events can be quite different from that of the signal events. The $0\nu\beta\beta$-decay events will be uniformly distributed throughout the source material, as will background events from $2\nu\beta\beta$ decay and other uniformly distributed radioactive sources. However, additional backgrounds will come from the mechanical support materials and localized detector components. Background events will be concentrated close to those nonactive materials. In experiments with discrete detectors, each detector may serve as a veto for other detectors in the system; multiple-scattered background γ-rays or $\beta\gamma$ decays are likely to deposit energy in more than one detector. In monolithic detectors, these background events may be rejected by an optimized fiducial volume cut. This configuration also enables the measurement of these backgrounds with high statistics, which can in turn be used as a constraint in the $0\nu\beta\beta$-decay analysis.

Many experiments use multiple variables to distinguish between signal and backgrounds. While this can be accomplished with hard cuts or a multidimensional fit, another option is to create an optimized discriminator variable based on machine learning techniques. In future searches, deep learning methods may also be applied to the problem of signal-to-background optimization (151).

Another technique that can distinguish $0\nu\beta\beta$ decay from all backgrounds other than $2\nu\beta\beta$ decay is the identification of the decay daughter on an event-by-event basis. The prototypical isotope for this technique is ^{136}Xe (152). The $\beta\beta$ decay of ^{136}Xe results in an ionized Ba daughter. This has been an intriguing system, with efforts by both the nEXO (153, 154) and NEXT (155) Collaborations to identify single Ba ions with high efficiency. This technique still presents significant

Table 2 $T^{0\nu}_{1/2}$ and $\langle m_{\beta\beta}\rangle$ limits (90% CL) from the most recent measurements, sorted by mass number

Isotope	$T^{0\nu}_{1/2}$ ($\times 10^{25}$ years)	$\langle m_{\beta\beta}\rangle$ (eV)	Experiment	Reference
^{48}Ca	$>5.8 \times 10^{-3}$	<3.5–22	ELEGANT-IV	159
^{76}Ge	>8.0	<0.12–0.26	GERDA	160
	>1.9	<0.24–0.52	Majorana Demonstrator	161
^{82}Se	$>3.6 \times 10^{-2}$	<0.89–2.43	NEMO-3	162
^{96}Zr	$>9.2 \times 10^{-4}$	<7.2–19.5	NEMO-3	163
^{100}Mo	$>1.1 \times 10^{-1}$	<0.33–0.62	NEMO-3	164
^{116}Cd	$>2.2 \times 10^{-2}$	<1.0–1.7	Aurora	165
^{128}Te	$>1.1 \times 10^{-2}$	NE	C. Arnaboldi et al.	166
^{130}Te	>1.5	<0.11–0.52	CUORE	126
^{136}Xe	>10.7	<0.061–0.165	KamLAND-Zen	167
	>1.8	<0.15–0.40	EXO-200	168
^{150}Nd	$>2.0 \times 10^{-3}$	<1.6–5.3	NEMO-3	169

The $\langle m_{\beta\beta}\rangle$ limits are listed as reported in refereed publications. Other unpublished preliminary results are described in the text. Abbreviation: NE, not evaluated.

challenges to implementation, but the implications for positive identification of a $\beta\beta$ decay and the background rejection capabilities are significant enough to motivate continued development for deployment in future experiments.

5. THE EXPERIMENTAL PROGRAM

Since the first direct searches for $0\nu\beta\beta$ decays were performed (156–158) in the 1960s, the experiments have grown from deploying grams to hundreds of kilograms of decay isotopes. As these detectors become more sophisticated—from reducing the overall backgrounds to improving the signal detection efficiency—the $T^{0\nu}_{1/2}$ limit has also improved from $\sim 10^{20}$ years to $\gtrsim 10^{26}$ years.

Much experimental progress has been made since the publication of the last $0\nu\beta\beta$-decay review in this journal (14). **Table 2** summarizes the current lower limits in $T^{0\nu}_{1/2}$ and $\langle m_{\beta\beta}\rangle$ for the different $\beta\beta$-decay isotopes. Note that there are many possible mechanisms for $0\nu\beta\beta$ decay (see Section 2.3); only the $\langle m_{\beta\beta}\rangle$ limits in the light-neutrino model are summarized in the table. **Figure 5** shows two influential detector parameters (Equation 15), energy resolution and background index, for some of the past, current, and future experiments. We have witnessed a tremendous amount of progress in background reduction, but formidable challenges to further improvement lie ahead. In the rest of this section, we discuss the detector technologies and the experimental program that are being pursued for the discovery of $0\nu\beta\beta$ decay.

5.1. Semiconductors

Among the different semiconductor detector technologies, ^{76}Ge-enriched high-purity germanium (HPGe) detectors are among the most auspicious for scaling to a tonne-scale experiment. The advent of using HPGe detectors in γ-ray spectroscopy and the network of commercial manufacturers have propelled this technology to a mature state. Other semiconductor technologies, such as CdZnTe (170) or a recent idea of a complementary metal-oxide-semiconductor (CMOS) pixel array (171), are still in an early feasibility study stage and are unlikely to be realized as a next-generation tonne-scale experiment.

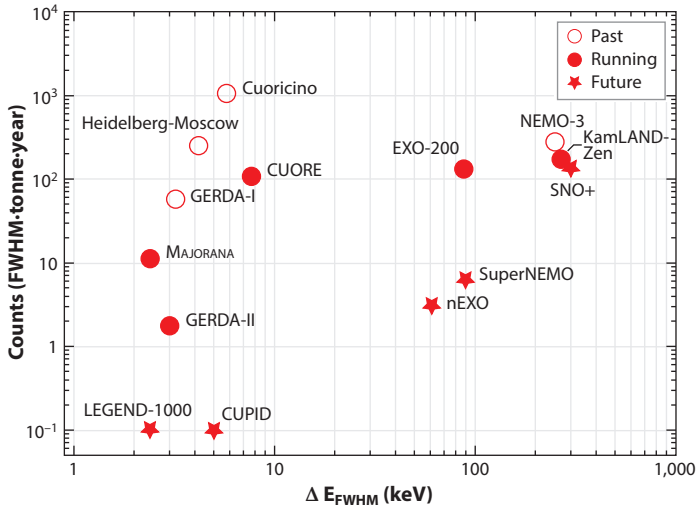

Figure 5

The background index as a function of full-width-at-half-maximum (FWHM) energy resolution for selected past, current, and future experiments with ^{76}Ge, ^{100}Mo, ^{130}Te, and ^{136}Xe as target. Note that large homogeneous detectors such as SNO+, KamLAND-Zen, and nEXO are not well characterized by a single background index.

The use of HPGe detectors in $0\nu\beta\beta$-decay searches offers several advantages. They are intrinsically clean, as impurities are removed in the detector crystal-growing process. They can be fabricated with ^{76}Ge-enriched materials; this source-as-detector configuration enhances the signal detection efficiency. They have superior energy resolution; in fact, an energy resolution of 0.12% (FWHM) at $Q_{\beta\beta}$ has been attained (161). However, HPGe detectors must be fabricated and installed individually, which complicates the scaling up to a larger array.

A number of advances in HPGe detector design have occurred since the last generation of ^{76}Ge experiments, Heidelberg–Moscow (172) and IGEX (173). The current generation of experiments—GERDA (174) and MAJORANA DEMONSTRATOR (175)—uses point-contact-type HPGe detectors (176, 177) that have good discrimination power between single-site signal and multisite background events. These detectors also have very low capacitance, allowing sensitive probe of New Physics, such as dark matter searches, at energies much lower than $Q_{\beta\beta}$ (178).

5.1.1. ^{76}Ge: GERDA. The Germanium Detector Array (GERDA) experiment (174) is located at the Laboratori Nazionali del Gran Sasso (LNGS) in L'Aquila, Italy. Bare 86%-enriched ^{76}Ge HPGe detectors are immersed in a liquid-Ar cryostat to minimize the amount of nearby mechanical components and high-Z shielding. In its first phase, GERDA-I, 17.8 kg of the enriched coaxial detectors from the Heidelberg–Moscow and IGEX experiments were initially deployed and were augmented by 3.63 kg in five broad energy Ge (BEGe) p-type point-contact detectors about halfway through data taking. After accumulating an exposure of 21.6 kg·year of data from late 2011 to mid-2013, the GERDA-I results (179) refuted the controversial claim of a 4.2σ significance of observing $0\nu\beta\beta$ decay in ^{76}Ge (150). An upgrade (180) prior to the second phase, GERDA-II, improved the radioactivity backgrounds and their rejection, as well as increasing the total enriched detector mass to 35.8 kg, of which BEGe detectors constituted 20 kg. The background improvements include the installation of a scintillating nylon shroud to shield the detectors from ^{42}K in the liquid Ar; ^{42}K is a progeny of ^{42}Ar and has a maximum β energy of 3,525 keV (181).

An efficient active veto, coupled with effective pulse-shape discrimination algorithms (182, 183) to reject multisite and α-background events, enabled GERDA-II to achieve an unprecedentedly low background index of $(1.0^{+0.6}_{-0.4}) \times 10^{-3}$ count (keV kg·year)$^{-1}$ (160). Combining the results from both phases, GERDA achieved a lower limit of $T^{0\nu}_{1/2}$ at 8.0×10^{25} years (90% CL). The median sensitivity assuming null signal was 5.8×10^{25} years.

In mid-2018, further improvements to the scintillation-light detection efficiency and the overall performance of the HPGe detectors were implemented. The GERDA Collaboration installed five enriched inverted coax point-contact (ICPC) detectors (184) with a total mass of 9 kg; these ICPC detectors are a promising candidate for future ^{76}Ge $0\nu\beta\beta$-decay experiments.

5.1.2. ^{76}Ge: Majorana Demonstrator. The Majorana Demonstrator (MJD) experiment (175) is operating 29.7 kg of 88%-enriched ^{76}Ge and 14.4 kg of natural p-type point-contact detectors at the 4,850-foot level of the Sanford Underground Research Facility (185) in Lead, South Dakota.

Unlike the GERDA experiment, the MJD experiment opted for a traditional arrangement in which the detectors are installed in two Cu vacuum cryostats, which are encapsulated in a graded shield consisting of layers of Cu, Pb, an active muon veto, polyethylene, and borated polyethylene. The whole setup is enclosed in a Rn exclusion box. The experiment relied on using ultraclean materials and process control (186) to reach the background objectives. For example, the Cu used in the cryostat, small parts near the detectors, and the innermost Cu shield were electroformed (129) and machined in the underground cleanroom to prevent contamination and cosmogenic activation.

The MJD experiment has been taking data since 2015, when only the first of two cryostats was populated with enriched detectors and the construction of the graded shield was just beginning. The construction was fully complete by early 2017. The MJD Collaboration has released the $0\nu\beta\beta$-decay search results for these different experimental configurations. With an integrated exposure of 26 kg·year in the latest data release, the collaboration obtained a lower limit of $T^{0\nu}_{1/2}$ at 2.7×10^{25} years (90% CL) with a median sensitivity of 4.8×10^{25} years (187). The measured energy resolution is 2.53 ± 0.08 keV (FWHM), and the background index in the lowest-background experimental configuration is $(4.7 \pm 0.8) \times 10^{-3}$ count (keV·kg·year)$^{-1}$. Similar to the GERDA analysis, pulse-shape discrimination techniques to identify and reject multisite events (188) and α backgrounds (189) were implemented.

5.1.3. ^{76}Ge: LEGEND. The GERDA and MJD results have demonstrated the technical feasibility of building a large-scale ^{76}Ge-based $0\nu\beta\beta$-decay experiment with ultralow background and superior energy resolution. The Large Enriched Germanium Experiment for Neutrinoless Double-Beta Decay (LEGEND) Collaboration was recently formed to pursue a tonne-scale ^{76}Ge-based experiment (190). The project will combine the strengths of the two operating experiments—low-Z shielding and scintillating veto for background suppression from GERDA and ultrapure materials and components from MJD—to attempt a $T^{0\nu}_{1/2}$ discovery sensitivity of $\sim 10^{28}$ years in a phased program.

In the first phase, LEGEND-200, the GERDA experimental infrastructure at LNGS will be modified and repurposed to accommodate up to approximately 200 kg of ^{76}Ge-enriched detectors. The $T^{0\nu}_{1/2}$ discovery potential for LEGEND-200 is expected to be $\sim 10^{27}$ years with a background index of 0.6 count (FWHM·tonne·year)$^{-1}$, a factor of $\sim$5 reduction from that in GERDA. As of early 2019, LEGEND-200 has been nearly fully funded, and the operation is anticipated to start in 2021. To reach the ultimate discovery potential at $T^{0\nu}_{1/2} \sim 10^{28}$ years, the background index in

the 1,000 kg of detectors in the subsequent phase, LEGEND-1000, needs to be further reduced to $\lesssim$0.1 count (FWHM·tonne·year)$^{-1}$.

5.2. Bolometers

The bolometric technique was first proposed for $0\nu\beta\beta$-decay searches in 1984 (191). Bolometers are cryogenic calorimeters that operate at temperatures of ∼10 mK. An absorber is connected to a low-temperature thermal bath via a weak thermal link, and the temperature is read out by a sensitive thermometer.

Bolometer absorbers can be grown from a wide variety of materials, including multiple $\beta\beta$-decay isotopes. Examples of these crystals include TeO_2 (natural or enriched in ^{130}Te), $^{116}CdWO_4$, $Zn^{82}Se$, $^{40}Ca^{100}MoO_4$, $Zn^{100}MoO_4$, and $Li_2^{100}MoO_4$. Similar to semiconductor detectors, crystalline bolometers can be intrinsically low in radioactivity because of the crystal growth process. Readers are referred to Reference 192 for a comprehensive review of the use of bolometers in $\beta\beta$-decay experiments.

The typical rise in temperature is of the order of ∼0.1 mK per MeV of deposited energy. Highly sensitive thermometers such as neutron-transmutation-doped (NTD) Ge or Si, transition-edge sensors (TES), metallic magnetic calorimeters (MMC), and kinetic inductance detectors (KID) are used for reading out such minuscule temperature changes. The NTD Ge thermistors are the most widely used in $0\nu\beta\beta$-decay searches. In future bolometer-based experiments, the TES and KID devices will become more important, as they can be used to detect the Cherenkov or scintillation light due to radioactive backgrounds in the crystals, thus allowing the associated event to be rejected.

Excellent counting statistics in the phonon channel imply that bolometers should have energy resolution comparable to that of semiconductor detectors. They are inherently segmented arrays of crystals, like the semiconductor detectors, and therefore do not benefit dramatically from self-shielding as detector size increases. The challenge of working at extremely low temperatures increases the technical difficulty of building large detectors.

5.2.1. ^{130}Te: CUORE. The Cryogenic Underground Observatory for Rare Events (CUORE) experiment is located at LNGS. It consists of a close-packed array of 988 5×5×5 cm^3, 750-g TeO_2 absorber crystals arranged into 19 towers and cooled to 7 mK by a powerful dilution refrigerator. Like the MiDBD, Cuoricino (193), and CUORE-0 (194) experiments that preceded it, the CUORE experiment uses unenriched Te, taking advantage of the large natural abundance of ^{130}Te (195). The absorbers are instrumented with NTD Ge thermistors that are read out continuously. Each crystal is also outfitted with a heater for thermal gain stabilization, and further calibration is provided by γ-ray sources deployed between the towers. The array is surrounded by layers of γ-ray and neutron shielding, including low-background ancient Roman Pb shields in the cryogenic volume. Additional Pb, borated polyethylene, and boric acid are located outside the cryostat for further shielding.

The first $0\nu\beta\beta$-decay search results from the CUORE experiment, based on two month-long runs for a total exposure of 24.0 kg·year of ^{130}Te, set a limit of $T_{1/2}^{0\nu} > 1.3 \times 10^{25}$ years (90% CL) with a median sensitivity of 7.0×10^{24} years (126). In combination with the previous results from Cuoricino and CUORE-0, the limit becomes $T_{1/2}^{0\nu} > 1.5 \times 10^{25}$ years (90% CL). The experiment has achieved an energy resolution of 7.7 ± 0.5 keV (FWHM), or 0.30%, at $Q_{\beta\beta}$ and a background of 0.014 ± 0.002 count (keV·kg·year)$^{-1}$. The projected sensitivity of the CUORE experiment is 9×10^{25} years after 5 years of running (196).

5.2.2. ^{82}Se/^{100}Mo/^{130}Te: CUPID. While the CUORE detector reads out a single energy signal and therefore has minimal background discrimination capabilities, the CUORE Upgrade with Particle Identification (CUPID) Collaboration is exploring bolometer development to improve signal purity through active particle identification (197), particularly the discrimination of the dominant α backgrounds in CUORE (198). One approach is to detect the Cherenkov light from the β signal in TeO_2 (199). The use of ^{130}Te-enriched bolometers would further extend the reach of this CUPID configuration.

Another approach is to deploy scintillating bolometers to differentiate α particles, such as the $Zn^{82}Se$ crystals in CUPID-0 (200) or the $Zn^{100}MoO_4$ and $Li_2^{100}MoO_4$ crystals in the LUMINEU experiment (201, 202). CUPID-Mo, an experiment evolved from LUMINEU, has been running 20 ^{100}Mo-enriched, 0.2-kg $Li_2^{100}MoO_4$ crystals in the cryogenic setup of the EDELWEISS dark matter experiment at Laboratoire Souterrain de Modane (LSM) in the Fréjus Tunnel near Modane, France (202). Additional detectors will be deployed in the CUPID-0 setup at LNGS in 2019. The outcome of these research and development efforts will decide the best technology for the tonne-scale CUPID program that has the goals of a background index of ∼0.1 count (ROI·tonne·year)$^{-1}$ and of $T_{1/2}^{0\nu} > 10^{27}$ years (203).

5.2.3. ^{100}Mo: AMoRE. The Advanced Molybdenum Based Rare Process Experiment (AMoRE) is a ^{100}Mo-based experiment at the Yangyang Underground Laboratory (Y2L) in South Korea. It comprises $CaMoO_4$ scintillating crystals that are depleted to ∼0.002% in ^{48}Ca but enriched to ∼95% in ^{100}Mo (204). Metallic magnetic calorimeter sensors are used to read out the phonon signals. One of the two MMC sensors on each crystal is coupled to an Au film on a Ge wafer. The phonons generated from the light absorbed in the wafer are collected by the Au film and measured by the attached sensor via a superconducting quantum interference device (SQUID). AMoRE-Pilot, the pilot phase of the project, has been operating since 2015. AMoRE-I and AMoRE-II, the next phases of the project with ∼5 kg of $^{48\text{depl}}Ca^{100}MoO_4$ crystals and ∼200 kg of ^{100}Mo-based crystals, are projected to reach a $T_{1/2}^{0\nu}$ sensitivity of $\sim 10^{25}$ years and $\sim 5 \times 10^{26}$ years, respectively (205).

5.3. Time-Projection Chambers

The time-projection chamber (TPC) is an attractive detector technology for $0\nu\beta\beta$-decay searches because of a combination of mass scalability and access to multiple background discrimination variables. A TPC takes advantage of a detection medium that produces two energy channels: ionization and scintillation. The combination of these two signals enables the reconstruction of event topology, position, and energy. The ionization-to-scintillation ratio provides convenient particle discrimination between α particles (high recombination leading to low ionization to scintillation) and γ-rays or β electrons (low recombination leading to relatively high ionization to scintillation). For $0\nu\beta\beta$-decay searches, ^{136}Xe-enriched xenon is a convenient source and detection medium. Xe TPCs can be built for both gas and liquid phases. By operating high-pressure gas-phase Xe TPCs in electroluminescent mode, an energy resolution of better than 0.5% FWHM at $Q_{\beta\beta}$ can be achieved (206).

Liquid-phase Xe TPCs offer maximum source density. Two-phase liquid-Xe detectors are popular for dark matter searches. These experiments—LUX-ZEPLIN (207) and XENON-nT (208), which are under construction, and the future DARWIN (209) project—might have the capability to search for $0\nu\beta\beta$ decay. In fact, DARWIN aims at a $T_{1/2}^{0\nu}$ sensitivity of 8.5×10^{27} years (90% CL) for a natural Xe exposure of 140 tonne·year, which is comparable to dedicated tonne-scale $0\nu\beta\beta$-decay experiments.

Rather than optimizing for a low energy threshold as in dark matter detectors, liquid-phase Xe TPCs for $0\nu\beta\beta$-decay searches are optimized for low-radioactive-background construction and energy resolution, resulting in the choice of single-phase detectors. The achievable energy resolution is somewhat worse than that of gas-phase detectors. While scattering prevents the resolution of the two β tracks, multisite background and spatial distribution discrimination work well, with position resolution achievable at the few-millimeter level.

5.3.1. ^{136}Xe: EXO-200. EXO-200 (210), a prototype of the Enriched Xenon Observatory (EXO) project, was located at the Waste Isolation Pilot Plant near Carlsbad, New Mexico. The cylindrical single-phase liquid-Xe TPC was filled with an active mass of 110 kg of Xe, enriched to 80.6% in ^{136}Xe, at a temperature of 167 K (210). EXO-200 employed a central cathode with detector planes at both ends consisting of crossed-wire grids for ionization collection and large-area avalanche photodiodes for scintillation collection. The low-mass Cu vessel for Xe containment was surrounded by HFE-700 cooling and shielding fluid within a double-walled Cu cryostat, which in turn was inside 25 cm of low-background Pb shielding with an active muon veto. An extensive screening program was undertaken to select detector materials (132, 133). In addition, EXO-200 analysis employs a multidimensional approach to background discrimination, including spatial and topological information, as well as particle discrimination.

EXO-200 data taking proceeded in two phases. Phase I began taking data with enriched Xe in 2011 and reported the first observation of $2\nu\beta\beta$ decay in ^{136}Xe (211). EXO-200 has produced a precision measurement of the $2\nu\beta\beta$-decay half-life, demonstrating the power of the liquid-Xe TPC technique (212). Phase I ended because of an unrelated fire and radiation release at the experimental site in early 2014. The experiment was upgraded with a Rn suppression system and low-noise electronics. Data taking restarted for Phase II in 2016 and completed in 2018. The first results from Phase II gave a $T^{0\nu}_{1/2}$ limit of 1.8×10^{25} years (90% CL) (168). The current EXO-200 detector performance displays an energy resolution of 2.90% (FWHM) at $Q_{\beta\beta}$ and a background index of $(1.6 \pm 0.2) \times 10^{-3}$ (keV·kg·year)$^{-1}$ in the $\pm 2\sigma$ ROI. Final analysis of the full EXO-200 data set is in progress.

5.3.2. ^{136}Xe: nEXO. nEXO is a planned tonne-scale single-phase liquid-Xe TPC based on the success of EXO-200 (213). The TPC will contain 5,000 kg of Xe enriched to 90% in ^{136}Xe. With lower-noise silicon photomultipliers (SiPMs) for scintillation collection, the expected energy resolution will be 2.4% (FWHM) at $Q_{\beta\beta}$. Multiple underground locations for hosting the nEXO experiment have been studied, including the SNOLAB Cryopit (214). The projected $T^{0\nu}_{1/2}$ sensitivity for the experiment is approximately 10^{28} years with a 3σ discovery potential of 5.7×10^{27} years (215). At this sensitivity and with the projected energy resolution, the $2\nu\beta\beta$-decay background is negligible. The power of this detector comes from having a large monolithic source volume, good energy resolution, and the background discrimination capabilities of a TPC. The low-background materials and construction techniques needed to achieve this sensitivity are not beyond what has already been demonstrated by current experiments.

5.3.3. ^{136}Xe: NEXT. The Neutrino Experiment with a Xenon TPC (NEXT) is a planned high-pressure gas-phase Xe TPC that employs amplification via electroluminescence to achieve an energy resolution of <1% (FWHM) at $Q_{\beta\beta}$ (216). NEXT-100, which will deploy 100 kg of enriched Xe at 15 bar, will be located at the Laboratorio Subterráneo de Canfranc (LSC) in Spain. At this pressure, individual β tracks can be resolved, including increased energy deposition at the end of the track where the electron becomes nonrelativistic. This distinctive topological signature for $\beta\beta$-decay events can be used to reject other sources of background.

An array of photomultiplier tubes (PMTs) detects both the primary scintillation light and the secondary scintillation light to reconstruct the event energy, and a second array of SiPMs located near the amplification region is used for track reconstruction. Tracking allows background rejection through the identification of individual β energy depositions in the detector. Initial studies estimate that a signal efficiency of 28% and a background rate of 4×10^{-4} count (keV·kg·year)$^{-1}$ are achievable. The NEXT-100 detector is projected to reach a $T^{0\nu}_{1/2}$ sensitivity of 2.8×10^{25} years (90% CL) after 3 years of running.

5.3.4. ^{136}Xe: PandaX-III. The Particle and Astrophysical Xenon Experiment III (PandaX-III), located at the China Jinping Underground Laboratory II (CJPL-II), is a high-pressure gas-phase TPC for $0\nu\beta\beta$-decay search in ^{136}Xe (217). Its first phase will feature one 200-kg TPC module operated at a pressure of 10 bar. The next phase will consist of five upgraded modules, bringing the experiment to the tonne scale. Charges are read out by microbulk micromegas (MM) modules (218) that line the endcaps of the cylindrical vessel. The expected energy resolution and background index for the 200-kg module are 3% (FWHM) at $Q_{\beta\beta}$ and $\sim 10^{-4}$ count (keV·kg·year)$^{-1}$ in the ROI, respectively. The projected $T^{0\nu}_{1/2}$ sensitivity is 10^{26} years after 3 years of running. With an improved energy resolution of 1% (FWHM) and a lower background index of $\sim 10^{-5}$ count (keV·kg·year)$^{-1}$, the tonne-scale PandaX-III would reach a $T^{0\nu}_{1/2}$ sensitivity of 10^{27} years after 3 years.

5.4. Organic Scintillators

Although organic scintillators do not have superior energy resolution, their main appeal as a $0\nu\beta\beta$-decay detector is the mass scalability. Unlike other $0\nu\beta\beta$-decay experiments with solid targets, contaminants in the liquid scintillator may be removed online. The $\beta\beta$-decay isotope can be removed during circulation as well, allowing possible systematic checks of rate scaling in the event of a discovery.

Liquid scintillators typically have two components: solvents that form the bulk and fluors with an emission spectrum that better matches the response of the photodetectors as a dopant. The popular choices of solvents in previous large-scale neutrino experiments were pseudocumene and dodecane; for instance, KamLAND (Kamioka Liquid Scintillator Antineutrino Detector) used a 20:80 by volume mix of the two solvents. A solvent that is gaining popularity in recent years is linear alkylbenzene (LAB) (219). This solvent offers a high flash point, low toxicity, high compatibility with most materials, and low cost. A common choice for fluor in $\beta\beta$-decay experiments is PPO (2,5-diphenyloxazole). Both KamLAND-Zen (Zero Neutrino) (^{136}Xe) and SNO+ (^{130}Te) experiments use this wavelength-shifting agent.

As discussed in Section 4.2, the irreducible background of solar neutrinos scattering off atomic electrons is problematic for large liquid-scintillator detectors. These elastic scattering events have strong directionality and are correlated to the Sun's direction. The key to mitigate this background is to separate the directional Cherenkov light emitted by the relativistic electrons from the isotropic scintillation light that has a much higher intensity. In bench measurements, the CHESS (220) and FlatDot (221) experiments have recently demonstrated the separability of the prompt Cherenkov and the delayed scintillation light through timing in LAB-based scintillators. These encouraging results could lead to the realization of much larger detectors for $0\nu\beta\beta$-decay searches, such as the proposed 50-kilotonne THEIA detector (222).

5.4.1. ^{136}Xe: KamLAND-Zen and KamLAND2-Zen. Using the KamLAND infrastructure at the Kamioka Observatory in Gifu Prefecture, Japan, the KamLAND-Zen experiment searches for $0\nu\beta\beta$ decay in ^{136}Xe. Various amounts of ^{136}Xe, enriched to 90%, were at different times

loaded in a liquid-scintillator cocktail of 82% decane and 18% pseudocumene by volume, along with 2.7 g L^{-1} of PPO as fluor. This Xe-loaded liquid scintillator (Xe-LS) is contained in a 25-μm-thick nylon miniballoon, suspended in liquid scintillator at the center of the 13-m-diameter main balloon. The main balloon is installed in an 18-m-diameter stainless steel spherical vessel, which is filled with a nonscintillating buffer oil. On the vessel, 1,879 17-inch and 20-inch PMTs, combined into a photocathode coverage of 34%, are mounted. A 3.2-kilotonne cylindrical water Cherenkov detector outside the containment vessel serves as a muon veto.

In phase I of KamLAND-Zen 400, 320 kg of enriched Xe were loaded. A dominant background from ^{110m}Ag β decay, believed to be the fallout from the Fukushima incident in 2011, limited the sensitivity of the experiment (223). The Xe-LS was subsequently purified over 1.5 years, and the contamination was successfully reduced by an order of magnitude prior to the commencement of phase II. Various event selection criteria, including Bi-Po time coincidence and a fiducial volume limited to a radial distance of 2 m from the center of the detector, were used to improve the signal-to-noise ratio in the signal region of interest. With 380 kg of enriched Xe and a total exposure of 504 kg·year in phase II, the KamLAND-Zen 400 experiment obtained a $T^{0\nu}_{1/2}$ lower limit of 1.07×10^{26} years (90% CL) and a median sensitivity of 5.6×10^{25} years (167).

Detailed background studies in phase II identified contaminations on the surface of the miniballoon, as well as residual ^{110m}Ag in the liquid scintillator. An arduous effort to purify the liquid scintillator and to remake the balloon ensued at the end of phase II running. The KamLAND-Zen Collaboration has completed the installation of a new miniballoon, and loading of 750 kg of enriched Xe in this new phase of KamLAND-Zen 800 experiment is imminent.

In the longer term, the KamLAND-Zen Collaboration plans to deploy over a tonne of enriched Xe and to reduce the $2\nu\beta\beta$-decay background in the signal ROI by improving the detector resolution in the KamLAND2-Zen experiment. Research and development of various strategies to increase the amount of detected scintillation light—from increasing the light yield with a different liquid scintillator to increasing the light collection with light concentrators and improving the detection efficiency with PMTs that have higher quantum efficiency—are being conducted. Background reduction and rejection studies, involving the development of new techniques in ^{10}C rejection and the fabrication of a scintillating mini-balloon, are in progress as well. If the goal of improving the energy resolution by a factor of two is attained, KamLAND2-Zen may reach a $T^{0\nu}_{1/2}$ sensitivity of $\sim 2 \times 10^{27}$ years after 5 years of running.

5.4.2. ^{96}Zr: ZICOS. The Zirconium Complex in Liquid Scintillator (ZICOS) experiment (224) is a new effort to dissolve a high concentration of tetrakis (isopropyl acetoacetate) zirconium [$Zr(iprac)_4$] in liquid scintillator. The collaboration is investigating the properties of the liquid scintillator, including the ability to separate the Cherenkov and scintillation light from ^{208}Tl $\beta - \gamma$ decay. Preliminary design studies indicate that ~45 kg of ^{96}Zr enriched to 50% could reach a $T^{0\nu}_{1/2}$ lower limit of 2×10^{26} years; the ability to reject ^{208}Tl $\beta - \gamma$ background in situ would improve the limit to $\sim 10^{27}$ years.

5.5. Inorganic Scintillators

With a high $Q_{\beta\beta}$ of 4.27 MeV, inorganic CaF_2 scintillators have been attracting interest from experimenters since the early days of $0\nu\beta\beta$-decay searches. The $\beta\beta$-decay isotope ^{48}Ca is amalgamated in the scintillator crystal-growing process. The primary background in a ^{48}Ca experiment is no longer the 2,615-keV γ-ray from ^{208}Tl; instead, the more penetrating γ-rays from (n, γ) radiative capture in the containment vessel and the rock surrounding the crystals are the most significant (225). These high-energy γ-rays can be either shielded by passive shielding

or identified by an active veto, or both. The most challenging aspect of a ^{48}Ca experiment is to find a cost-effective way to enrich the isotope, whose natural abundance is only 0.187%. A recent tabletop experiment has demonstrated a significant enrichment ratio using multichannel countercurrent electrophoresis (226); this breakthrough has the potential to produce significant quantities of ^{48}Ca at a much lower cost than other traditional enrichment techniques.

5.5.1. ^{48}Ca: CANDLES. The CANDLES series (227) of $0\nu\beta\beta$-decay searches in ^{48}Ca is being carried out at the Kamioka Observatory. In the latest CANDLES-III setup, 96 natural CaF_2 scintillator crystals with a total mass of 305 kg are suspended from the roof of a 2-m^3 liquid-scintillator vessel. Scintillation light from both the inorganic crystals and the liquid scintillator is observed by 62 PMTs via light pipes. The PMTs are mounted in a 3-m-diameter, 4-m-tall cylindrical water tank. The experiment recently reported preliminary results from 131 live days of data (226). Contamination from Th up to ~60 μBq kg^{-1} was observed in some of the crystals. For those crystals with a Th contamination of <10 μBq kg^{-1}, there is no candidate event in the signal region of interest, resulting in a $T^{0\nu}_{1/2}$ lower limit of 6.2×10^{22} years (90% CL) and a median sensitivity of 3.6×10^{22} years.

5.6. Tracking Calorimeters

Tracking calorimeters take a multilayered detection approach. Rather than distributing the source throughout the detector volume, tracking calorimeters such as NEMO-3 (228) and SuperNEMO (49) use a thin foil of source material in the center of a sandwich configuration, surrounded first by a low-pressure gas tracking layer to track the two β particles and then a calorimetric layer to measure the energy. This type of detector provides superior topological information and is the only detector technology capable of measuring the opening angle between the two β particles—one observable that can distinguish certain underlying mechanisms for $0\nu\beta\beta$ decay (Section 2.3). In addition, many different isotopes can be formed into foils and studied in the same detector configuration. Background discrimination is excellent, but the thin source foils are difficult to scale up to large exposure.

SuperNEMO (229, 230) is a next-generation detector based on the technology demonstrated by NEMO-3 (228), which successfully studied multiple $0\nu\beta\beta$ isotopes including ^{100}Mo. The NEMO program is unique in that the $\beta\beta$-decay source material is distinct from the detection medium, allowing multiple isotopes to be studied with a single detector configuration. A demonstrator module for SuperNEMO is under construction at the LSM. This module contains 6.3 kg of ^{82}Se in 34 foils, surrounded by a tracking detector made up of drift cells operating in Geiger mode. Operating in a magnetic field of 25 G, the tracking detector allows for the identification of the two β particles for both background rejection and the measurement of angular correlations. The tracking detector is surrounded on four sides by calorimetry planes consisting of blocks of scintillator read out by PMTs. The planned energy resolution of the detector is 4% (FWHM) at 3 MeV, the $Q_{\beta\beta}$ of ^{82}Se. The demonstrator module will reach a $T^{0\nu}_{1/2}$ sensitivity of $>5.85 \times 10^{24}$ years (90% CL) after 2.5 years of running. For a full SuperNEMO detector consisting of 20 modules, the sensitivity to the half-life of ^{82}Se is projected to be 1.2×10^{26} years.

6. CONCLUSIONS

We have described the most recent theoretical and experimental development in $0\nu\beta\beta$ decay. If discovered, this lepton-number-violating process would have profound implications for our understanding of the evolution of the Universe and the fundamental theory of elementary particles.

In the light-neutrino exchange mechanism, neutrino mass limits approaching the projected mass-scale sensitivity of the KATRIN experiment are around the corner. Tests of the inverted-ordering regime are crucial for the standard neutrino paradigm, and those in the range of normal ordering are even more so. Beyond the light-neutrino regime, there are various plausible mechanisms spanning a multitude of energy scales, including those accessible at present and future colliders, that could mediate $0\nu\beta\beta$ decay. This implies interesting tests of the mechanisms and investigations of the so-called inverse problem of the decay, that is, identifying the origin of the decay once it is observed. The nuclear and hadronic aspects of $0\nu\beta\beta$ decay remain challenges for precise physics extraction from an experimental limit or a possible signal. In the development of new theoretical approaches, new aspects of these problems are routinely being discovered. These are signs of a vibrant field and give hope that those uncertainties will become much smaller in the near future.

On the experimental side, this is an exciting time to search for $0\nu\beta\beta$ decay, the only realistic direct probe for lepton-number violation. Since the first direct searches in the 1960s, the $T^{0\nu}_{1/2}$ limit has improved by six orders of magnitude, reaching $\gtrsim 10^{26}$ years in the current generation of experiments. These experiments feature the deployment of different $\beta\beta$-decay isotopes and detector technologies, enabling numerous advancements in isotope preparation, clean-material development, radioactivity mitigation, signal detection, and analysis.

Well-motivated half-life predictions are within experimental reach. The next generation of $0\nu\beta\beta$-decay searches offers the potential of a discovery at $T^{0\nu}_{1/2}$ exceeding 10^{28} years. To realize this goal, these experiments will have to be able to achieve the formidable background index of $\lesssim 0.1$ count (FWHM·tonne·year)$^{-1}$ in a robust tonne-scale detector that is expected to operate with a high duty cycle for a decade or longer. Despite these challenges, international teams are spearheading efforts to mount at least one of these experiments, projecting to reach the intermediate $T^{0\nu}_{1/2}$ discovery potential of $\sim 10^{27}$ years in the coming decade.

DISCLOSURE STATEMENT

The authors are not aware of any affiliations, memberships, funding, or financial holdings that might be perceived as affecting the objectivity of this review.

ACKNOWLEDGMENTS

We thank Brian Fujikawa, Wick Haxton, Martin Hirsch, and Tadafumi Kishimoto for helpful discussions. We are grateful for Ralph Massarczyk's help in producing **Figure 5**. M.J.D. is partially supported by the US Department of Energy (DOE), Office of Science, Office of Nuclear Physics, under award DE-SC0014517 to Drexel University. W.R. is supported by the Deutsche Forschungsgemeinschaft with grant RO 2516/7-1 in the Heisenberg Programme. Lawrence Berkeley National Laboratory is operated by the Regents of the University of California for the US DOE under Federal Prime Agreement DE-AC02-05CH11231.

LITERATURE CITED

1. Fukuda Y, et al. *Phys. Rev. Lett.* 81:1562 (1998)
2. Ahmad QR, et al. *Phys. Rev. Lett.* 89:011301 (2002)
3. Eguchi K, et al. *Phys. Rev. Lett.* 90:021802 (2003)
4. Kajita T. *Rev. Mod. Phys.* 88:030501 (2016)
5. McDonald AB. *Rev. Mod. Phys.* 88:030502 (2016)

6. Majorana E. *Nuovo Cim.* 14:171 (1937)
7. Schechter J, Valle JWF. *Phys. Rev. D* 25:2951 (1982)
8. Goeppert-Mayer M. *Phys. Rev.* 48:512 (1935)
9. Inghram MG, Reynolds JH. *Phys. Rev.* 78:822 (1950)
10. Elliott SR, Hahn AA, Moe MK. *Phys. Rev. Lett.* 59:2020 (1987)
11. Moe M. *Annu. Rev. Nucl. Part. Sci.* 64:247 (2014)
12. Saakyan R. *Annu. Rev. Nucl. Part. Sci.* 63:503 (2013)
13. Moe M, Vogel P. *Annu. Rev. Nucl. Part. Sci.* 44:247 (1994)
14. Elliott SR, Vogel P. *Annu. Rev. Nucl. Part. Sci.* 52:115 (2002)
15. Rodejohann W. *Int. J. Mod. Phys. E* 20:1833 (2011)
16. Dell'Oro S, Marcocci S, Viel M, Vissani F. *Adv. High Energy Phys.* 2016:2162659 (2016)
17. Kotila J, Iachello F. *Phys. Rev. C* 85:034316 (2012)
18. Stoica S, Mirea M. *Phys. Rev. C* 88:037303 (2013)
19. Balantekin AB, Kayser B. *Annu. Rev. Nucl. Part. Sci.* 68:313 (2018)
20. Parno D. Talk presented at the 28th International Conference on Neutrino Physics and Astrophysics, Heidelberg, Ger., June 4–9. **https://doi.org/10.5281/zenodo.1287933** (2018)
21. Gastaldo L. Talk presented at the 28th International Conference on Neutrino Physics and Astrophysics, Heidelberg, Ger., June 4–9. **https://doi.org/10.5281/zenodo.1286949** (2018)
22. Lattanzi M, Gerbino M. *Front. Phys.* 5:70 (2018)
23. Aghanim N, et al. arXiv:1807.06209 [astro-ph.CO] (2018)
24. Sprenger T, et al. arXiv:1801.08331 [astro-ph.CO] (2018)
25. Brinckmann T, et al. arXiv:1808.05955 [astro-ph.CO] (2018)
26. Ashtari Esfahani A, et al. *J. Phys. G* 44:054004 (2017)
27. Pascoli S, Petcov ST. *Phys. Lett. B* 544:239 (2002)
28. Esteban I, et al. arXiv:1811.05487 [hep-ph] (2018)
29. Hannestad S, Schwetz T. *J. Cosmol. Astropart. Phys.* 1611:035 (2016)
30. Schwetz T, et al. arXiv:1703.04585 [astro-ph.CO] (2017)
31. Gariazzo S, et al. *J. Cosmol. Astropart. Phys.* 1803:011 (2018)
32. Caldwell A, Merle A, Schulz O, Totzauer M. *Phys. Rev. D* 96:073001 (2017)
33. Agostini M, Benato G, Detwiler J. *Phys. Rev. D* 96:053001 (2017)
34. Ge SF, Rodejohann W, Zuber K. *Phys. Rev. D* 96:055019 (2017)
35. Maltoni M. Talk presented at the 28th International Conference on Neutrino Physics and Astrophysics, Heidelberg, Ger., June 4–9. **https://doi.org/10.5281/zenodo.1287015** (2018)
36. Giunti C, Lasserre T. arXiv:1901.08330 [hep-ph] (2019)
37. Helo JC, Hirsch M, Ota T. *J. High Energy Phys.* 06:006 (2016)
38. Keung WY, Senjanovic G. *Phys. Rev. Lett.* 50:1427 (1983)
39. Helo JC, Hirsch M, Kovalenko S. *Phys. Rev. D* 89:073005 (2014). Erratum. *Phys. Rev. D* 93:099902 (2016)
40. Antusch S, Cazzato E, Fischer O. *Int. J. Mod. Phys. A* 32:1750078 (2017)
41. Nemevek M, Nesti F, Popara G. *Phys. Rev. D* 97:115018 (2018)
42. Lindner M, Queiroz FS, Rodejohann W, Yaguna CE. *J. High Energy Phys.* 06:140 (2016)
43. Biswal SS, Dev PSB. *Phys. Rev. D* 95:115031 (2017)
44. Deppisch FF, Bhupal Dev PS, Pilaftsis A. *New J. Phys.* 17:075019 (2015)
45. Cai Y, Han T, Li T, Ruiz R. *Front. Phys.* 6:40 (2018)
46. Hirsch M, Klapdor-Kleingrothaus HV, Panella O. *Phys. Lett. B* 374:7 (1996)
47. Barry J, Rodejohann W. *J. High Energy Phys.* 09:153 (2013)
48. Cirigliano V, et al. *J. High Energy Phys.* 12:097 (2018)
49. Arnold R, et al. *Eur. Phys. J. C* 70:927 (2010)
50. Helo JC, Hirsch M, Pas H, Kovalenko SG. *Phys. Rev. D* 88:073011 (2013)
51. Peng T, Ramsey-Musolf MJ, Winslow P. *Phys. Rev. D* 93:093002 (2016)
52. Frere JM, Hambye T, Vertongen G. *J. High Energy Phys.* 01:051 (2009)
53. Deppisch FF, Harz J, Hirsch M. *Phys. Rev. Lett.* 112:221601 (2014)
54. Duerr M, Lindner M, Merle A. *J. High Energy Phys.* 06:091 (2011)

55. Pas H, Hirsch M, Klapdor-Kleingrothaus HV, Kovalenko SG. *Phys. Lett. B* 498:35 (2001)
56. Graf L, Deppisch FF, Iachello F, Kotila J. *Phys. Rev. D* 98:095023 (2018)
57. Deppisch FF, Hirsch M, Pas H. *J. Phys. G* 39:124007 (2012)
58. Meroni A, Petcov ST, Simkovic F. *J. High Energy Phys.* 02:025 (2013)
59. González M, Hirsch M, Kovalenko SG. *Phys. Rev. D* 93:013017 (2016). Erratum. *Phys. Rev. D* 97:099907 (2018)
60. Mahajan N. *Phys. Rev. Lett.* 112:031804 (2014)
61. Arbelez C, González M, Kovalenko S, Hirsch M. *Phys. Rev. D* 96:015010 (2017)
62. González M, Hirsch M, Kovalenko S. *Phys. Rev. D* 97:115005 (2018)
63. Cirigliano V, et al. *J. High Energy Phys.* 12:082 (2017)
64. Arbelez C, González M, Hirsch M, Kovalenko S. *Phys. Rev. D* 94:096014 (2016). Erratum. *Phys. Rev. D* 97:099904 (2018)
65. Long AJ, Lunardini C, Sabancilar E. *J. Cosmol. Astropart. Phys.* 1408:038 (2014)
66. Berryman JM, de Gouvêa A, Kelly KJ, Schmitt M. *Phys. Rev. D* 98:016009 (2018)
67. Yoshimura M. *Phys. Lett. B* 699:123 (2011)
68. Dinh DN, et al. *Phys. Lett. B* 719:154 (2013)
69. Millar A, Raffelt G, Stodolsky L, Vitagliano E. *Phys. Rev. D* 98:123006 (2018)
70. Rosen SP. *Phys. Rev. Lett.* 48:842 (1982)
71. Rodejohann W, Xu XJ, Yaguna CE. *J. High Energy Phys.* 05:024 (2017)
72. Dib CO, Kim CS. *Phys. Rev. D* 92:093009 (2015)
73. Winter RG. *Phys. Rev.* 100:142 (1955)
74. Bernabeu J, De Rujula A, Jarlskog C. *Nucl. Phys. B* 223:15 (1983)
75. Eliseev SA, Novikov YN, Blaum K. *J. Phys. G* 39:124003 (2012)
76. Eliseev S, Novikov YN, Blaum K. *Ann. Phys.* 525:707 (2013)
77. Graesser ML. *J. High Energy Phys.* 08:099 (2017)
78. Cirigliano V, Dekens W, Graesser M, Mereghetti E. *Phys. Lett. B* 769:460 (2017)
79. Prezeau G, Ramsey-Musolf M, Vogel P. *Phys. Rev. D* 68:034016 (2003)
80. Nicholson A, et al. *Proc. Sci.* LATTICE2016:017 (2016)
81. Shanahan PE, et al. *Phys. Rev. Lett.* 119:062003 (2017)
82. Nicholson A, et al. *Phys. Rev. Lett.* 121:172501 (2018)
83. Faessler A, Kovalenko S, Simkovic F, Schwieger J. *Phys. Rev. Lett.* 78:183 (1997)
84. Simkovic F, Pantis G, Vergados JD, Faessler A. *Phys. Rev. C* 60:055502 (1999)
85. Cirigliano V, et al. *Phys. Rev. Lett.* 120:202001 (2018)
86. Wang LJ, Engel J, Yao JM. *Phys. Rev. C* 98:031301 (2018)
87. Engel J, Menendez J. *Rept. Prog. Phys.* 80:046301 (2017)
88. Vergados JD, Ejiri H, Simkovic F. *Rept. Prog. Phys.* 75:106301 (2012)
89. Vergados JD, Ejiri H, Simkovic F. *Int. J. Mod. Phys. E* 25:1630007 (2016)
90. Rodriguez TR, Martinez-Pinedo G. *Phys. Rev. Lett.* 105:252503 (2010)
91. Lopez Vaquero N, Rodriguez TR, Egido JL. *Phys. Rev. Lett.* 111:142501 (2013)
92. Yao JM, et al. *Phys. Rev. C* 91:024316 (2015)
93. Rath PK, et al. *Phys. Rev. C* 82:064310 (2010)
94. Menendez J, Poves A, Caurier E, Nowacki F. *Nucl. Phys. A* 818:139 (2009)
95. Horoi M, Neacsu A. *Phys. Rev. C* 93:024308 (2016)
96. Iwata Y, et al. *Phys. Rev. Lett.* 116:112502 (2016). Erratum. *Phys. Rev. Lett.* 117:179902 (2016)
97. Barea J, Iachello F. *Phys. Rev. C* 79:044301 (2009)
98. Barea J, Kotila J, Iachello F. *Phys. Rev. C* 87:014315 (2013)
99. Barea J, Kotila J, Iachello F. *Phys. Rev. C* 91:034304 (2015)
100. Fang DL, Faessler A, Simkovic F. *Phys. Rev. C* 92:044301 (2015)
101. Mustonen MT, Engel J. *Phys. Rev. C* 87:064302 (2013)
102. Jokiniemi L, Ejiri H, Frekers D, Suhonen J. *Phys. Rev. C* 98:024608 (2018)
103. Pastore S, et al. *Phys. Rev. C* 97:014606 (2018)
104. Yao JM, et al. *Phys. Rev. C* 98:054311 (2018)

105. Faessler A, et al. *Phys. Rev. D* 79:053001 (2009)
106. Deppisch FF, Suhonen J. *Phys. Rev. C* 94:055501 (2016)
107. Suhonen J. *Front. Phys.* 5:55 (2017)
108. Frekers D, Puppe P, Thies JH, Ejiri H. *Nucl. Phys. A* 916:219 (2013)
109. Bodenstein-Dresler L, et al. arXiv:1806.02254 [nucl-ex] (2018)
110. Dell'Oro S, Marcocci S, Vissani F. *Phys. Rev. D* 90:033005 (2014)
111. Gando A, et al. arXiv:1901.03871 [hep-ex] (2019)
112. Simkovic F, Dvornicky R, Stefanik D, Faessler A. *Phys. Rev. C* 97:034315 (2018)
113. Menendez J, Gazit D, Schwenk A. *Phys. Rev. Lett.* 107:062501 (2011)
114. Engel J, Simkovic F, Vogel P. *Phys. Rev. C* 89:064308 (2014)
115. Ekstrom A, et al. *Phys. Rev. Lett.* 113:262504 (2014)
116. Frekers D, Alanssari M. *Eur. Phys. J. A* 54:177 (2018)
117. Freeman SJ, et al. *Phys. Rev. C* 75:051301 (2007)
118. Menendez J, Poves A, Caurier E, Nowacki F. *Phys. Rev. C* 80:048501 (2009)
119. Cappuzzello F, et al. *Eur. Phys. J. A* 54:72 (2018)
120. Shimizu N, Menendez J, Yako K. *Phys. Rev. Lett.* 120:142502 (2018)
121. Simkovic F, Smetana A, Vogel P. arXiv:1808.05016 [nucl-th] (2018)
122. Cappuzzello F, et al. *Eur. Phys. J. A* 51:145 (2015)
123. Hashim IH, et al. *Phys. Rev. C* 97:014617 (2018)
124. Berglund M, Wieser ME. *Pure Appl. Chem.* 83:397 (2011)
125. Tretyak VI, Zdesenko YG. *At. Data Nucl. Data Tables* 80:83 (2002)
126. Alduino C, et al. *Phys. Rev. Lett.* 120:132501 (2018)
127. Heusser G. *Annu. Rev. Nucl. Part. Sci.* 45:543 (1995)
128. Formaggio JA, Martoff CJ. *Annu. Rev. Nucl. Part. Sci.* 54:361 (2004)
129. Hoppe EW, et al. *Nucl. Instrum. Methods A* 764:116 (2014)
130. Suriano AM, et al. *AIP Conf. Proc.* 1921:080001 (2018)
131. Majorovits B, et al. *AIP Conf. Proc.* 1921:090001 (2018)
132. Leonard DS, et al. *Nucl. Instrum. Methods A* 591:490 (2008)
133. Leonard DS, et al. *Nucl. Instrum. Methods A* 871:169 (2017)
134. Abgrall N, et al. *Nucl. Instrum. Methods A* 828:22 (2016)
135. Loach JC, et al. *Nucl. Instrum. Methods A* 839:6 (2016)
136. Suzuki T, Measday DF, Roalsvig JP. *Phys. Rev. C* 35:2212 (1987)
137. Macdonald B, Diaz JA, Kaplan SN, Pyle RV. *Phys. Rev. B* 139:1253 (1965)
138. Heisinger B, et al. *Earth Planet. Sci. Lett.* 200:357 (2002)
139. Boswell MS, et al. *Phys. Rev. C* 87:064607 (2013)
140. Negret A, Borcea C, Plompen AJM. *Phys. Rev. C* 88:027601 (2013)
141. Wang BS, et al. *Phys. Rev. C* 92:024620 (2015)
142. Baudis L, Kish A, Piastra F, Schumann M. *Eur. Phys. J. C* 75:485 (2015)
143. Armengaud E, et al. *Astropart. Phys.* 91:51 (2017)
144. Ma JL, et al. *Sci. China Phys. Mech. Astron.* 62:11011 (2019)
145. Heisinger B, et al. *Earth Planet. Sci. Lett.* 200:345 (2002)
146. Cebrián S. *Int. J. Mod. Phys. A* 32:1743006 (2017)
147. Zhang C, Mei DM, Kudryavtsev VA, Fiorucci S. *Astropart. Phys.* 84:62 (2016)
148. Abe S, et al. *Phys. Rev. C* 81:025807 (2010)
149. Albert JB, et al. *J. Cosmol. Astropart. Phys.* 1604:029 (2016)
150. Klapdor-Kleingrothaus HV, Krivosheina IV, Dietz A, Chkvorets O. *Phys. Lett. B* 586:198 (2004)
151. Renner J, et al. *J. Instrum.* 12:T01004 (2017)
152. Moe MK. *Phys. Rev. C* 44:931 (1991)
153. Green M, et al. *Phys. Rev. A* 76:023404 (2007)
154. Chambers C, et al. arXiv:1806.10694 [physics.ins-det] (2018)
155. McDonald AD, et al. *Phys. Rev. Lett.* 120:132504 (2018)
156. der Mateosian E, Goldhaber M. *Phys. Rev.* 146:810 (1966)

157. Lazarenko VR, Luk'yanov SY. *Sov. Phys. JETP* 22:521 (1966)
158. Fiorini E, et al. *Phys. Lett. B* 25:602 (1967)
159. Umehara S, et al. *Phys. Rev. C* 78:058501 (2008)
160. Agostini M, et al. *Phys. Rev. Lett.* 120:132503 (2018)
161. Aalseth CE, et al. *Phys. Rev. Lett.* 120:132502 (2018)
162. Barabash AS, Brudanin VB. *Phys. At. Nucl.* 74:312 (2011)
163. Argyriades J, et al. *Nucl. Phys. A* 847:168 (2010)
164. Arnold R, et al. *Phys. Rev. D* 92:072011 (2015)
165. Barabash AS, et al. *Phys. Rev. D* 98:092007 (2018)
166. Arnaboldi C, et al. *Phys. Lett. B* 557:167 (2003)
167. Gando A, et al. *Phys. Rev. Lett.* 117:082503 (2016). Addendum. *Phys. Rev. Lett.*117:109903 (2016)
168. Albert JB, et al. *Phys. Rev. Lett.* 120:072701 (2018)
169. Arnold R, et al. *Phys. Rev. D* 94:072003 (2016)
170. Ebert J, et al. *Phys. Rev. C* 94:024603 (2016)
171. Chavarria AE, Galbiati C, Li X, Rowlands JA. *J. Instrum.* 12:P03022 (2017)
172. Klapdor-Kleingrothaus HV, et al. *Eur. Phys. J. A* 12:147 (2001)
173. Aalseth CE, et al. *Phys. Rev. D* 65:092007 (2002)
174. Ackermann KH, et al. *Eur. Phys. J. C* 73:2330 (2013)
175. Abgrall N, et al. *Adv. High Energy Phys.* 2014:365432 (2014)
176. Luke PN, Goulding FS, Madden NW, Pehl RH. *IEEE Trans. Nucl. Sci.* 36:926 (1989)
177. Barbeau PS, Collar JI, Tench O. *J. Cosmol. Astropart. Phys.* 0709:009 (2007)
178. Abgrall N, et al. *Phys. Rev. Lett.* 118:161801 (2017)
179. Agostini M, et al. *Phys. Rev. Lett.* 111:122503 (2013)
180. Agostini M, et al. *Eur. Phys. J. C* 78:388 (2018)
181. Lubashevskiy A, et al. *Eur. Phys. J. C* 78:15 (2018)
182. Agostini M, et al. *Eur. Phys. J. C* 73:2583 (2013)
183. Budjas D, et al. *J. Instrum.* 4:P10007 (2009)
184. Cooper R, et al. *Nucl. Instrum. Methods A* 665:25 (2011)
185. Lesko KT. *Phys. Proc.* 61:542 (2015)
186. Christofferson CD, et al. *AIP Conf. Proc.* 1921:060005 (2018)
187. Alvis SI, et al. arXiv:1902.02299 [nucl-ex] (2019)
188. Alvis SI, et al. arXiv:1901.05388 [physics.ins-det] (2019)
189. Gruszko J, et al. *J. Phys. Conf. Ser.* 888:012079 (2017)
190. Abgrall N, et al. *AIP Conf. Proc.* 1894:020027 (2017)
191. Fiorini E, Niinikoski TO. *Nucl. Instrum. Methods A* 224:83 (1984)
192. Poda D, Giuliani A. *Int. J. Mod. Phys. A* 32:1743012 (2017)
193. Arnaboldi C, et al. *Phys. Lett. B* 584:260 (2004)
194. Alduino C, et al. *J. Instrum.* 11:P07009 (2016)
195. Arnaboldi C, et al. *Nucl. Instrum. Methods A* 518:775 (2004)
196. Alduino C, et al. *Eur. Phys. J. C* 77:532 (2017)
197. Artusa DR, et al. *Phys. Lett. B* 767:321 (2017)
198. Wang G, et al. arXiv:1504.03599 [physics.ins-det] (2015)
199. Battistelli ES, et al. *Eur. Phys. J. C* 75:353 (2015)
200. Azzolini O, et al. *Phys. Rev. Lett.* 120:232502 (2018)
201. Barabash AS, et al. *Eur. Phys. J. C* 74:3133 (2014)
202. Poda DV. *AIP Conf. Proc.* 1894:020017 (2017)
203. Ouellet J. Talk presented at the 28th International Conference on Neutrino Physics and Astrophysics, Heidelberg, Ger., June 4–9. **https://doi.org/10.5281/zenodo.1286904** (2018)
204. Lee JY, et al. *IEEE Trans. Nucl. Sci.* 65:2041 (2018)
205. Kim S. Talk presented at the 28th International Conference on Neutrino Physics and Astrophysics, Heidelberg, Ger., June 4–9. **https://doi.org/10.5281/zenodo.1300715** (2018)
206. Alvarez V, et al. *J. Instrum.* 7:T06001 (2012)

207. Akerib DS, et al. arXiv:1509.02910 [physics.ins-det] (2015)
208. Aprile E. (Xenon Collab.) In *APS April Meeting Abstracts*. **https://meetings.aps.org/Meeting/APR17/Session/J9.7** (2017)
209. Aalbers J, et al. *J. Cosmol. Astropart. Phys.* 1611:017 (2016)
210. Auger M, et al. *J. Instrum.* 7:P05010 (2012)
211. Ackerman N, et al. *Phys. Rev. Lett.* 107:212501 (2011)
212. Albert JB, et al. *Phys. Rev. C* 89:015502 (2014)
213. Kharusi SA, et al. arXiv:1805.11142 [physics.ins-det] (2018)
214. Duncan F, Noble AJ, Sinclair D. *Annu. Rev. Nucl. Part. Sci.* 60:163 (2010)
215. Albert JB, et al. *Phys. Rev. C* 97:065503 (2018)
216. Martin-Albo J, et al. *J. High Energy Phys.* 05:159 (2016)
217. Han K. Talk presented at 15th International Conference on Topics in Astroparticle and Underground Physics, Sudbury, Can., July 24–28 (2017)
218. Andriamonje S, et al. *J. Instrum.* 5:P02001 (2010)
219. O'Keeffe HM, O'Sullivan E, Chen MC. *Nucl. Instrum. Methods A* 640:119 (2011)
220. Caravaca J, et al. *Phys. Rev. C* 95:055801 (2017)
221. Gruszko J, et al. arXiv:1811.11144 [physics.ins-det] (2018)
222. Orebi Gann GD. arXiv:1504.08284 [physics.ins-det] (2015)
223. Gando A, et al. *Phys. Rev. Lett.* 110:062502 (2013)
224. Fukuda Y. *J. Phys. Conf. Ser.* 718:062019 (2016)
225. Nakajima K, et al. *Astropart. Phys.* 100:54 (2018)
226. Kishimoto T. Talk presented at International Workshop on Double Beta Decay and Underground Science (DBD 2018), Waikoloa, HI, October 21–23 (2018)
227. Umehara S, et al. *Phys. Proc.* 61:283 (2015)
228. Arnold R, et al. *Nucl. Instrum. Methods A* 536:79 (2005)
229. Barabash AS, et al. *Nucl. Instrum. Methods A* 868:98 (2017)
230. Patrick C. Talk presented at International Workshop on Double Beta Decay and Underground Science (DBD 2018), Waikoloa, HI, October 21–23 (2018)